Crossover-active regions of the wheat genome are distinguished by DMC1, the chromosome axis, H3K27me3, and signatures of adaptation

Andrew J. Tock,[1,6] Daniel M. Holland,[1,6] Wei Jiang,[1] Kim Osman,[2] Eugenio Sanchez-Moran,[2] James D. Higgins,[3] Keith J. Edwards,[4] Cristobal Uauy,[5] F. Chris H. Franklin,[2] and Ian R. Henderson[1]

[1]*Department of Plant Sciences, University of Cambridge, Cambridge CB2 3EA, United Kingdom;* [2]*School of Biosciences, University of Birmingham, Birmingham B15 2TT, United Kingdom;* [3]*Department of Genetics and Genome Biology, University of Leicester, Leicester LE1 7RH, United Kingdom;* [4]*School of Biological Sciences, University of Bristol, Bristol BS8 1TQ, United Kingdom;* [5]*John Innes Centre, Norwich NR4 7UH, United Kingdom*

The hexaploid bread wheat genome comprises over 16 gigabases of sequence across 21 chromosomes. Meiotic crossovers are highly polarized along the chromosomes, with elevation in the gene-dense distal regions and suppression in the *Gypsy* retrotransposon-dense centromere-proximal regions. We profiled the genomic landscapes of the meiotic recombinase DMC1 and the chromosome axis protein ASY1 in wheat and investigated their relationships with crossovers, chromatin state, and genetic diversity. DMC1 and ASY1 chromatin immunoprecipitation followed by sequencing (ChIP-seq) revealed strong co-enrichment in the distal, crossover-active regions of the wheat chromosomes. Distal ChIP-seq enrichment is consistent with spatiotemporally biased cytological immunolocalization of DMC1 and ASY1 close to the telomeres during meiotic prophase I. DMC1 and ASY1 ChIP-seq peaks show significant overlap with genes and transposable elements in the *Mariner* and *Mutator* superfamilies. However, DMC1 and ASY1 ChIP-seq peaks were detected along the length of each chromosome, including in low-crossover regions. At the fine scale, crossover elevation at DMC1 and ASY1 peaks and genes correlates with enrichment of the Polycomb histone modification H3K27me3. This indicates a role for facultative heterochromatin, coincident with high DMC1 and ASY1, in promoting crossovers in wheat and is reflected in distalized H3K27me3 enrichment observed via ChIP-seq and immunocytology. Genes with elevated crossover rates and high DMC1 and ASY1 ChIP-seq signals are overrepresented for defense-response and immunity annotations, have higher sequence polymorphism, and exhibit signatures of selection. Our findings are consistent with meiotic recombination promoting genetic diversity, shaping host–pathogen co-evolution, and accelerating adaptation by increasing the efficiency of selection.

[Supplemental material is available for this article.]

Meiosis is a germ-line cell division whereby chromosomes undergo DNA replication followed by two rounds of segregation, producing gametes required for sexual reproduction (Villeneuve and Hillers 2001). Homologous chromosomes pair and recombine, yielding crossovers or noncrossovers (Hunter 2015). Crossovers are required for balanced segregation at the first division and generate genetic diversity. Recombination is initiated during early prophase I, when chromosomes undergo DNA double-strand breaks (DSBs) catalyzed by SPO11 enzymes (Keeney et al. 2014). DMC1 and RAD51 recombinases bind single-stranded DNA at each DSB end and promote strand invasion of homologous DNA (Hunter 2015). In plants and mammals, a minority of strand invasion events mature into crossovers (~3%–10% of DSBs) (Cole et al. 2010; Mercier et al. 2015), with most dissociated via anticrossover pathways (Hunter 2015).

Meiotic recombination is orchestrated by the assembly of a proteinaceous axis, which underpins meiotic chromosome architecture in eukaryotes (Zickler and Kleckner 1999). Sister chromatids are organized as linear arrays of chromatin loops connected to the axis (Zickler and Kleckner 1999). In plants, the chromosome axis includes the HORMA domain protein ASY1 and its interacting partners ASY3 and ASY4, which promote DMC1-mediated interhomolog synapsis and recombination (Armstrong et al. 2002; Sanchez-Moran et al. 2007; Ferdous et al. 2012; Chambon et al. 2018). As prophase I progresses, the synaptonemal complex is installed between the axes of homologous chromosomes, promoting crossover maturation (Zickler and Kleckner 1999).

Crossovers exert a powerful influence on eukaryotic genetic variation and genome evolution (Barton and Charlesworth 1998) and are an essential plant-breeding tool. However, significant heterogeneity in crossover rates occurs along chromosomes, which can impede crop improvement (Taagen et al. 2020). Selection for useful variation can cause hitchhiking of deleterious alleles via linkage drag in low-recombination regions (Hill and

[6]**These authors contributed equally to this work.**
Corresponding authors: irh25@cam.ac.uk, ajt200@cam.ac.uk
Article published online before print. Article, supplemental material, and publication date are at https://www.genome.org/cgi/doi/10.1101/gr.273672.120.

31:1614–1628 Published by Cold Spring Harbor Laboratory Press; ISSN 1088-9051/21; www.genome.org

Robertson 1966). This is particularly pronounced in bread wheat (*Triticum aestivum*), as crossovers concentrate in distal regions (Saintenac et al. 2009; Choulet et al. 2014). For example, 82% of crossovers on Chromosome 3B occur within 19% of its physical length (Darrier et al. 2017). Bread wheat is an allohexaploid, comprising homoeologous A, B, and D subgenomes of seven chromosomes each ($2n = 6x = 42$, AABBDD) (Marcussen et al. 2014). Wheat chromosomes are large (473–830 Mb), with high transposable element (TE) content, and comprise one of the most complex assembled genomes (IWGSC 2018).

Pronounced compartmentalization of features occurs along the wheat chromosomes. For example, crossover rate, gene density, and euchromatic (H3K4me3, H3K9ac, and H3K27ac) and facultative heterochromatic (H3K27me3) marks increase toward the telomeres, whereas *Gypsy* LTR retrotransposon density and constitutive heterochromatic marks (H3K9me2 and CG- and CHG-context DNA methylation) increase toward the centromeres (Choulet et al. 2014; IWGSC 2018; Li et al. 2019). Gene function, chromatin state, and expression breadth across tissues are also stratified (Ramírez-González et al. 2018). Genes with broad expression, high H3K36me3 and H3K9ac levels, and "housekeeping" functions are located predominantly in the low-recombination interstitial and centromere-proximal regions (R2 and C compartments), whereas those with tissue-specific expression, high H3K27me3 levels, and functions in development and response to environmental stimuli are enriched in the high-recombination distal regions (R1 and R3 compartments) (IWGSC 2018; Ramírez-González et al. 2018).

Chromatin state significantly influences recombination in plant genomes. For example, meiotic DSB hotspots in *Arabidopsis* and maize are located in nucleosome-depleted regions (NDRs) associated with genes and specific transposon families (He et al. 2017; Choi et al. 2018). Furthermore, *Arabidopsis* crossover hotspots can be suppressed via RNA-directed DNA methylation (Yelina et al. 2015), and mutants with reduced non-CG DNA methylation show increased pericentromeric SPO11-1-oligonucleotides and crossovers (Underwood et al. 2018). Large tracts of the crossover-suppressed compartments of the wheat genome are marked by constitutive heterochromatin (IWGSC 2018; Li et al. 2019; Concia et al. 2020). Additionally, H3K27me2 associates with crossover suppression in wheat, despite distal enrichment (Liu et al. 2021). However, fine-scale relationships between chromatin, meiotic recombination, axis occupancy, and sequence variation in wheat remain incompletely understood.

As DMC1 marks an early stage in meiotic recombination, and the axis protein ASY1 promotes synapsis and recombination, we sought to profile their localization in wheat using ChIP-seq. This allowed us to investigate the genetic and epigenetic features that associate with meiotic DSBs and axis occupancy. DMC1 binding and axis occupancy are necessary, but not sufficient, for repair of meiotic DSBs as crossovers. We therefore aimed to identify properties that distinguish crossover-active DMC1 and ASY1 ChIP-seq peaks and genes by examining chromatin state and genetic variation across crossover-rate gradients.

Results

DMC1 recombinase colocalizes with the meiotic axis protein ASY1

We used polyclonal antibodies raised against *Arabidopsis* DMC1 in rabbit (Sanchez-Moran et al. 2007) and the recombinant wheat ASY1 HORMA domain in guinea pig (Desjardins et al. 2020). We performed western blotting using these antibodies and detected a specific band of the expected size from wheat floral extracts in each case, following nuclei extraction (DMC1 = 38 kDa; ASY1 = 67 kDa) (Supplemental Fig. S1). For ChIP-seq, the landrace Chinese Spring was selected due to the availability of a high-quality genome assembly, extensive chromatin data sets, and a genetic map (Guo et al. 2016; IWGSC 2018; Li et al. 2019). We collected pre-emergence spikes, which were crosslinked using formaldehyde, followed by nuclei purification and ChIP-seq using α-DMC1 and α-ASY1 antibodies.

After deduplication and trimming, 185,448,819 of 218,747,974 (85%) DMC1 and 344,590,350 of 405,615,455 (85%) ASY1 ChIP-seq read pairs mapped with a best-scoring alignment to the Chinese Spring genome (Supplemental Table S1). We also performed ChIP-seq for euchromatic (H3K4me3) and constitutive heterochromatic (H3K9me2 and H3K27me1) marks and mapped nucleosome occupancy via micrococcal nuclease digestion and sequencing (MNase-seq), using Chinese Spring leaf tissue. We combined analysis of our data with published ChIP-seq data sets for H3K4me1, H3K9ac, H3K27ac, H3K27me3, H3K36me3, and CENH3, and whole-genome bisulfite sequencing maps of DNA methylation (Guo et al. 2016; IWGSC 2018; Li et al. 2019; Supplemental Table S1).

At the chromosome scale, we observed a strong positive correlation between DMC1 and ASY1 ChIP-seq signals ($\log_2$[ChIP/input]) in adjacent 1-Mb windows (genome-wide Spearman's r_s = 0.97), with co-enrichment in distal compartments (Fig. 1A,B; Supplemental Figs. S2–S9). Distal ChIP-seq enrichment is consistent with immunolocalization of DMC1 and ASY1, showing telomere-biased accumulation early in prophase I (Fig. 2A,B; Osman et al. 2021). DMC1 and ASY1 chromosome-scale profiles positively correlate with crossover rate (cM/Mb) derived from a Chinese Spring × Renan F_6 genetic map (genome-wide r_s = 0.80 and 0.75, respectively) (IWGSC 2018), as well as with gene density and markers of euchromatin (H3K4me1, H3K4me3, and H3K27ac) and facultative heterochromatin (H3K27me3) (Fig. 1A,B; Supplemental Figs. S2, S3, S10–S12; IWGSC 2018; Li et al. 2019). These trends are also evident when distal (R1 and R3) and interstitial (R2) compartments are analyzed separately (Supplemental Fig. S12A,B). H3K27me3 marks facultative heterochromatin and mediates tissue-specific silencing of genes that control development or environmental responses (Mozgova and Hennig 2015). Consistent with distalized H3K27me3 ChIP-seq signal (Supplemental Fig. S10), immunostaining for this mark during meiotic prophase I also revealed distal enrichment (Fig. 2C,D; Osman et al. 2021).

We examined broad-scale relationships between recombination and genes within different functional categories that are known to have contrasting distributions. DMC1, ASY1 and crossover rate each exhibit strong positive relationships with genes annotated with the "defense response" Gene Ontology (GO) term (Ramírez-González et al. 2018) and those encoding nucleotide-binding and leucine-rich repeat domain intracellular immune receptor proteins (*NLR* genes) (Fig. 1A,B; Supplemental Fig. S12A, B; Steuernagel et al. 2020). Defense-response and *NLR* genes are concentrated in H3K27me3-enriched distal compartments (Fig. 1A; Supplemental Figs. S2, S10). In contrast, orthologs of known meiotic genes and genes with meiosis-related GO annotations concentrate in interstitial and proximal compartments (Alabdullah et al. 2019) and show weaker correlations with DMC1, ASY1, and crossover rate (Fig. 1B).

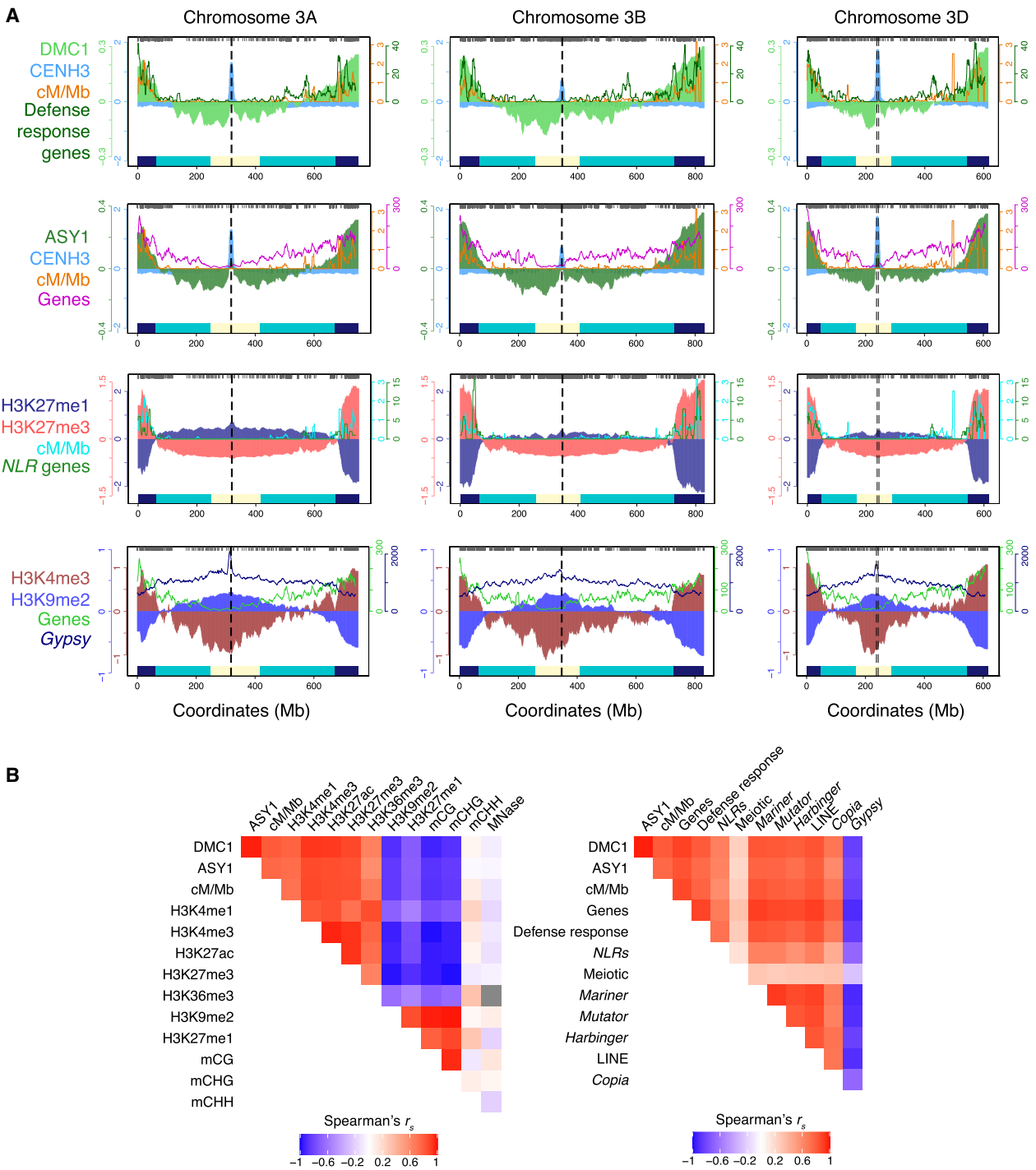

Figure 1. Genomic landscapes of DMC1 recombinase, the meiotic axis protein ASY1, crossovers, and chromatin states in wheat. (*A*) Coverage profiles along a representative set of homoeologous chromosomes (3A, 3B, and 3D) for DMC1 (light green), ASY1 (dark green), CENH3 (light blue) (Guo et al. 2016), H3K27me3 (red) (IWGSC 2018) (all $\log_2$[ChIP/input], using a Chinese Spring chromatin input sequencing library with accession SRR6350669) (IWGSC 2018), H3K27me1 (navy), H3K4me3 (dark red), and H3K9me2 (blue) (all $\log_2$[ChIP/MNase], using a Chinese Spring MNase-seq library from this study) ChIP-seq in 1-Mb adjacent windows, smoothed by applying a moving average. ChIP-seq chromosome profiles (shading) are overlaid with crossover rates (cM/Mb, derived from a Chinese Spring × Renan genetic map) (IWGSC 2018), and gene and *Gypsy* LTR retrotransposon frequencies in 10-Mb sliding windows with a 1-Mb step (lines). A representative set of the IWGSC RefSeq v1.1 Chinese Spring annotation of high-confidence protein-coding gene models (IWGSC 2018), genes annotated with the "defense response" Gene Ontology (GO) term (Ramírez-González et al. 2018), genes encoding nucleotide-binding and leucine-rich repeat (NLR) proteins (Steuernagel et al. 2020), and *Gypsy* LTR retrotransposons in the IWGSC annotation (IWGSC 2018) were plotted. Previously defined coordinates delimiting distal (R1 and R3, navy boxes), interstitial (R2a and R2b, turquoise boxes), proximal (C, cream boxes), and centromeric (vertical dashed lines) regions are indicated along the *x*-axis (IWGSC 2018). Gray ticks denote genomic coordinates of genetic markers used to construct the Chinese Spring × Renan genetic map. (*B*) Genome-wide Spearman's rank-order correlation coefficients (r_s) for the indicated parameter pairs profiled in 1-Mb adjacent windows, with cells coded according to the color-gradient correlation scale. Gray boxes denote correlation coefficients that are not significant after *P*-value standardization.

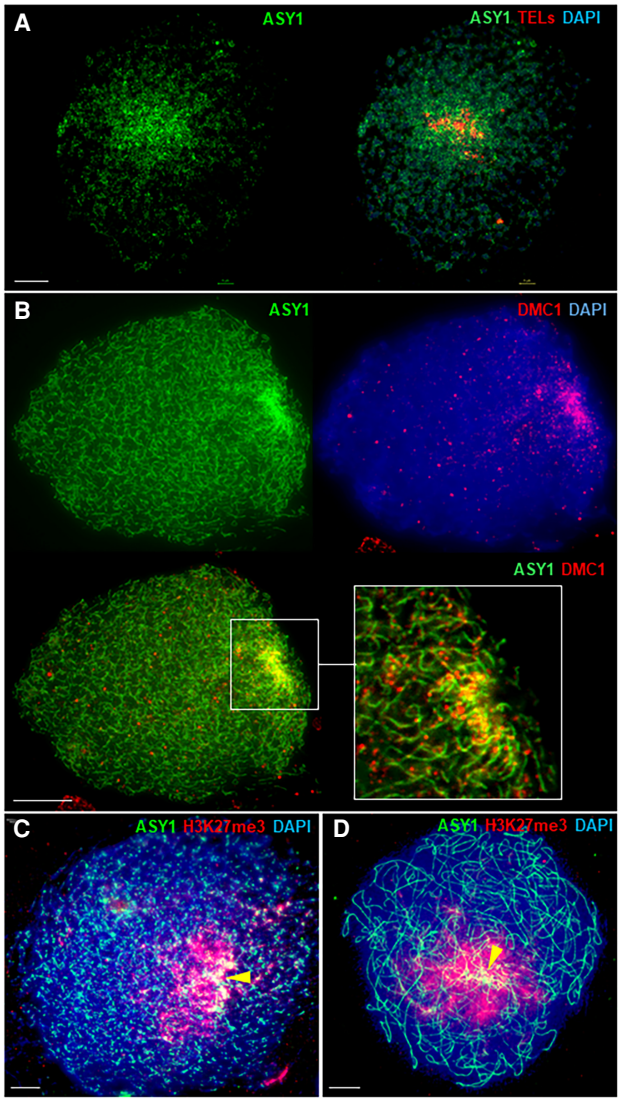

Figure 2. Immunolocalization of ASY1, DMC1, and H3K27me3 in pollen mother cells of wheat cultivar Cadenza during prophase I. (*A*) Immunolocalization of the axis protein ASY1 (green), combined with fluorescence in situ hybridization (FISH) of the telomeric repeat sequence (TELs, red) from *Arabidopsis thaliana* at the G2/leptotene transition. ASY1 signal is enriched in distal regions as the telomeres begin to cluster into a "bouquet" arrangement and the axis begins to linearize. (*B*) Leptotene-stage pollen mother cell immunostained for DMC1 foci (red) and co-immunostained for ASY1 (green), as axis linearization progresses through the nucleus. The zoomed detail of distal regions is from a single Z-frame (mid-nucleus) and shows individual DMC1 foci decorating the axis stained by ASY1. (*C*) Early-leptotene-stage pollen mother cell showing enrichment of H3K27me3 in distal regions, which are also marked by intense ASY1 immunostaining (yellow arrow). (*D*) H3K27me3 distal enrichment persists in early zygotene when chromosome axes are fully linear (yellow arrow). 4′,6-diamidino-2-phenylindole (DAPI) marks DNA. Scale bars = 10 µM. For clarity, some images are shown in several color combinations.

DMC1 and ASY1 peaks associate with genes and TIR DNA transposons

We identified sites of local DMC1 and ASY1 enrichment by calling peaks in ChIP-seq signal. For DMC1, 101,076 peaks were identified in distal (R1 and R3) compartments and 170,649 peaks in interstitial and proximal (R2 and C) compartments (Fig. 3A). For ASY1, 185,260 peaks were detected in distal compartments, and 358,946 peaks in interstitial and proximal compartments (Fig. 3B). We observed higher DMC1 and ASY1 peak densities in distal compartments, similar to chromosome-scale profiles for crossover rate, genes, and *Mariner* and *Mutator* transposons (Fig. 3C,D).

To investigate DMC1 and ASY1 peak properties, we evaluated their overlap with other features using permutation tests, each utilizing 10,000 sets of randomly positioned loci. In each set of subgenomic compartments, DMC1 peaks significantly overlap ASY1 peaks and vice versa (each $P = 0.0001$) (Fig. 3E; Supplemental Tables S2, S3). DMC1 and ASY1 peaks also significantly overlap ChIP-seq peaks for euchromatic histone modifications (H3K4me1, H3K9ac, H3K27ac, and H3K36me3) and facultative heterochromatin (H3K27me3), whereas they are largely absent from sites occupied by the constitutive heterochromatic mark H3K9me2 and LTR retrotransposons (Fig. 3E,F; Supplemental Tables S2, S3). Furthermore, DMC1 and ASY1 peaks significantly overlap DNA TEs containing terminal inverted repeats (TIRs), including the *Mariner* and *Mutator* superfamilies (each $P = 0.0001$) (Fig. 3F; Supplemental Tables S2, S3).

DMC1 and ASY1 peaks overlap genes more than expected and these associations are strongest in promoter regions upstream of transcriptional start sites (TSSs) and around transcriptional termination sites (TTSs) (each $P = 0.0001$) (Fig. 3E; Supplemental Tables S2, S3). Additionally, DMC1 and ASY1 peaks exhibit less-than-expected overlap with sites of high nucleosome occupancy (MNase-seq peaks) (Fig. 3E; Supplemental Tables S2, S3), consistent with elevated meiotic DSBs and crossovers in NDRs of *Arabidopsis*, tomato, and maize genes (Demirci et al. 2017; He et al. 2017; Choi et al. 2018; Fuentes et al. 2020). Multiple AT-rich sequences are overrepresented among DMC1 and ASY1 peaks (Supplemental Figs. S13, S14). AT sequence richness reduces nucleosome occupancy and promotes meiotic DSB and crossover formation in plant genomes (Shilo et al. 2015; Demirci et al. 2017; Choi et al. 2018; Fuentes et al. 2020). Despite positive chromosome-scale associations, DMC1 and ASY1 peaks overlap H3K4me3 peaks significantly less than expected (Fig. 3E; Supplemental Tables S2, S3). This is consistent with wheat meiotic DSBs and axis occupancy avoiding the +1 nucleosome at gene 5′ ends, which is modified with H3K4me3. These trends are reminiscent of *Arabidopsis* SPO11-1-oligos, which are also most enriched in NDRs flanking genes and depleted at the +1 nucleosome (Choi et al. 2018).

Crossover-active DMC1 and ASY1 peaks are distinguished by H3K27me3

DMC1 binding and axis occupancy are not sufficient for resolution of meiotic DSBs as crossovers, which is reflected in the detection of DMC1 and ASY1 peaks throughout all genomic compartments, including in crossover-suppressed regions. Therefore, we next sought to identify properties that associate with crossover-rate variation across DMC1 and ASY1 ChIP-seq peaks located in distal and interstitial/proximal compartments. We defined four groups of distal ChIP-seq peaks according to decreasing crossover rate, derived from the Chinese Spring × Renan genetic map (IWGSC 2018) (Quantiles 1–4; mean peaks per quantile: DMC1 = 24,634, ASY1 = 45,249) (Fig. 4A,B). Due to the smaller range of cM/Mb values in the recombination-suppressed compartments, peaks in these regions were divided into three groups (mean peaks per quantile: DMC1 = 56,883, ASY1 = 119,649) (Supplemental Fig. S15A,B).

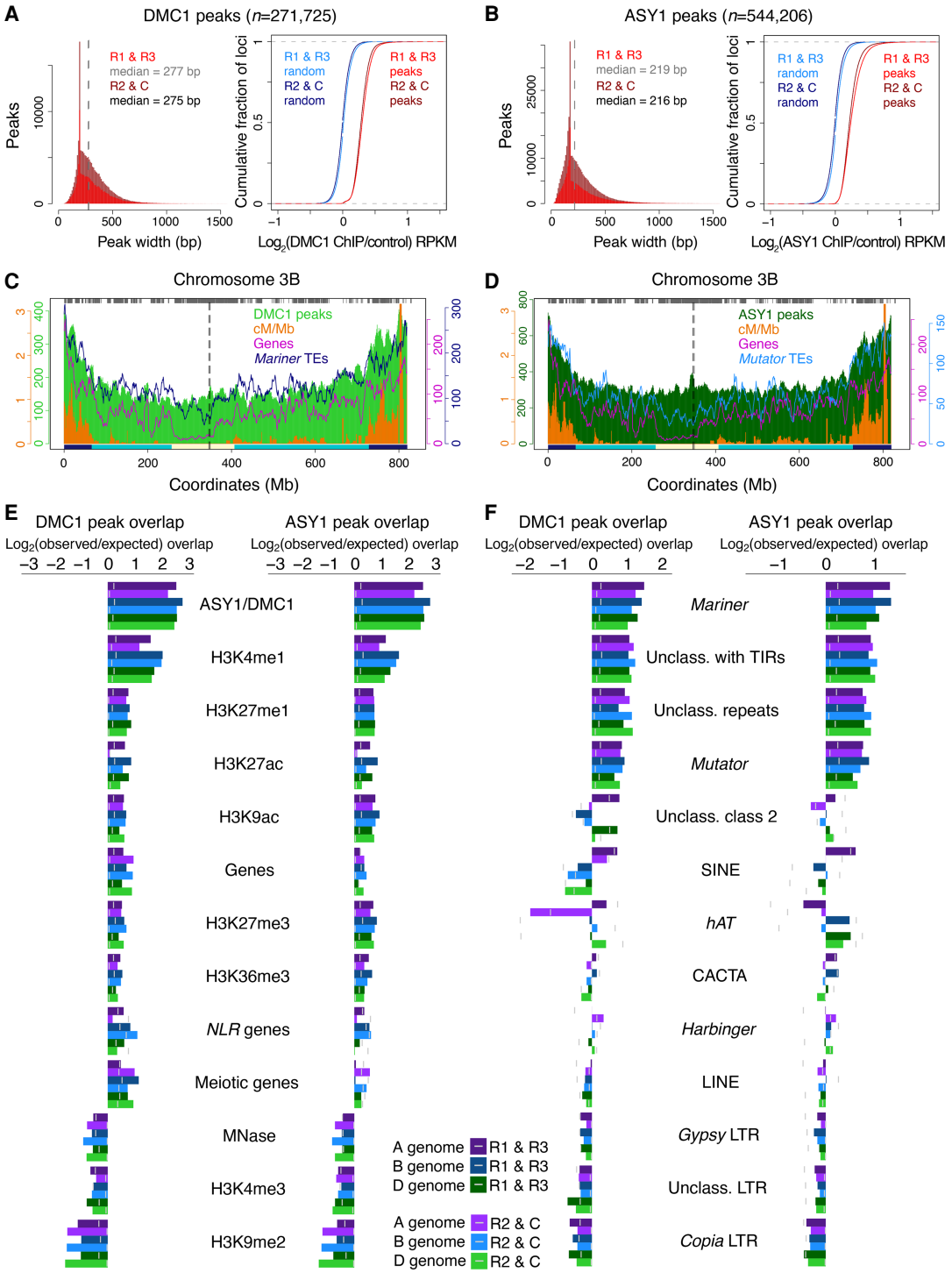

Figure 3. DMC1 and ASY1 ChIP-seq peaks associate with markers of euchromatin and heterochromatin. (*A*) Histograms of DMC1 ChIP-seq peak widths (bp) in distal compartments (R1 and R3, red) and in interstitial and proximal compartments (R2 and C, burgundy), with median widths indicated by vertical dashed lines in gray and black, respectively. Also shown are cumulative distribution curves for compartmentalized DMC1 ChIP-seq peaks and randomly positioned loci ranked by $\log_2$(ChIP/input) RPKM values. (*B*) As in *A*, but for ASY1 ChIP-seq peaks and randomly positioned loci. (*C*) Chromosome 3B profiles of DMC1 ChIP-seq peak frequencies (light green shading), crossover rate (cM/Mb, orange shading) (IWGSC 2018), gene frequency (magenta line), and *Mariner* transposon frequency (navy line) in 10-Mb sliding windows with a 1-Mb step. Previously defined coordinates delimiting distal (R1 and R3, navy boxes), interstitial (R2a and R2b, turquoise boxes), proximal (C, cream boxes), and centromeric (vertical dashed lines) regions are indicated along the *x*-axis (IWGSC 2018). Gray ticks denote genetic markers used to construct the Chinese Spring × Renan genetic map. (*D*) As in *C*, but showing ASY1 ChIP-seq peak frequency (dark green shading) and *Mutator* transposon frequency (light blue line). (*E*) $\log_2$(observed/expected) overlap of compartmentalized DMC1 and ASY1 ChIP-seq peaks in each subgenome with the indicated genomic features, based on the numbers of feature-overlapping loci across 10,000 sets of randomly positioned loci. Vertical gray lines mark significance thresholds ($\alpha = 0.05$). (*F*) As in *E*, but showing $\log_2$(observed/expected) overlap of DMC1 and ASY1 ChIP-seq peaks with transposon superfamilies.

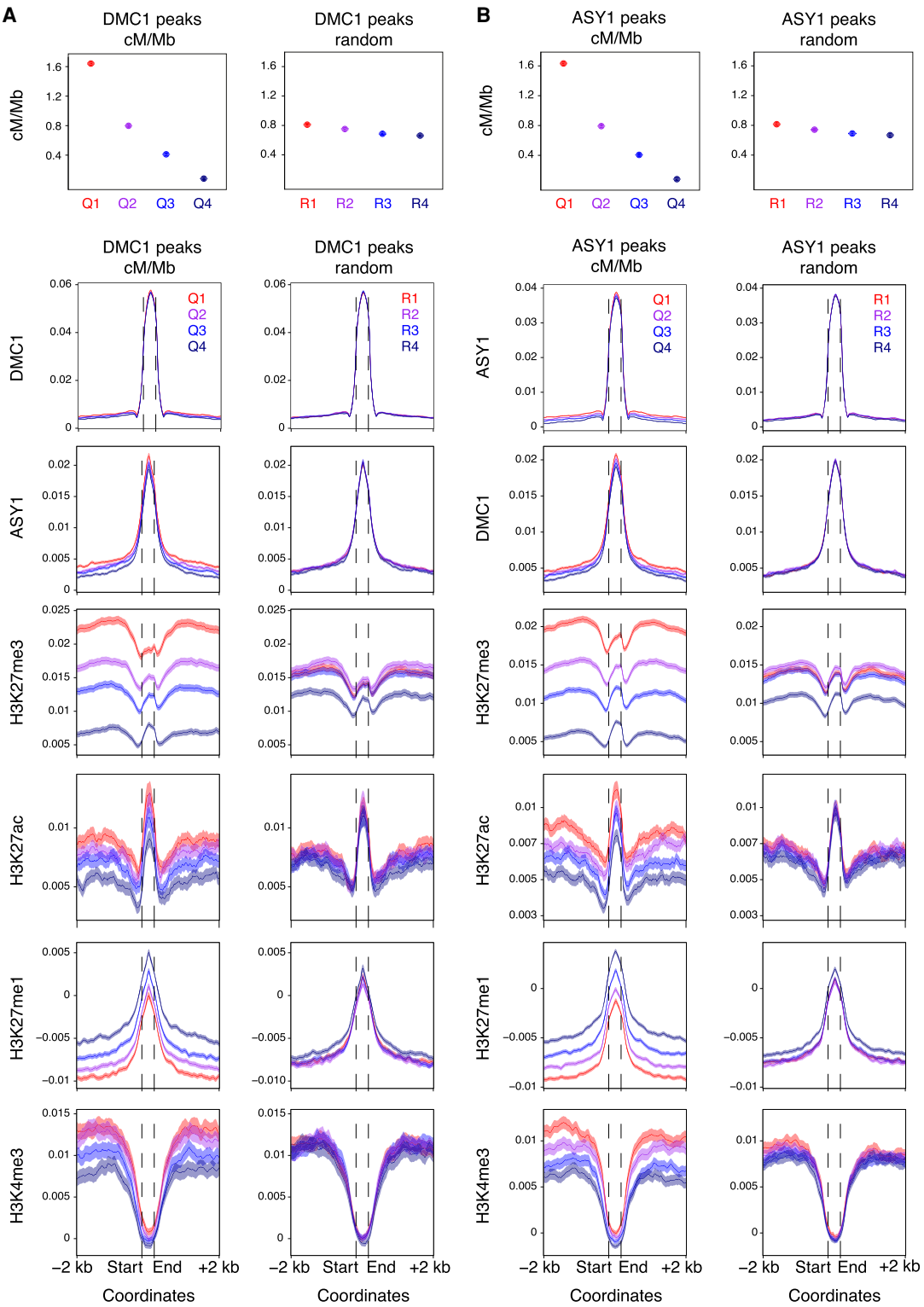

Figure 4. High-crossover-rate DMC1 and ASY1 ChIP-seq peaks are enriched for the Polycomb chromatin mark H3K27me3. (*A*) Distally located (R1 and R3) DMC1 ChIP-seq peaks were divided into four groups corresponding to those in the 100th–75th (Quantile 1), 75th–50th (Quantile 2), 50th–25th (Quantile 3), and 25th–0th (Quantile 4) percentiles with regard to their mean crossover rate (cM/Mb, derived from the Chinese Spring × Renan genetic map) between 1 kb upstream of peak start coordinates and 1 kb downstream from peak end coordinates (Q1–Q4, *left*), or into four randomized groups (R1–R4, *right*). Solid circles denote the mean crossover rate for each group of peaks (error bars = 95% confidence intervals for mean cM/Mb values). Metaprofiles show windowed mean values (solid lines) for each group of peaks and 2-kb flanking regions (transparent ribbons = 95% confidence intervals). ChIP-seq coverage metaprofiles of DMC1, ASY1, H3K27me3 (IWGSC 2018), and H3K27ac (Li et al. 2019) are derived from $\log_2$(ChIP/input) profiles, and those for H3K27me1 and H3K4me3 from $\log_2$(ChIP/MNase) profiles. (*B*) As in *A*, but for distal ASY1 ChIP-seq peaks.

DMC1 and ASY1 ChIP-seq metaprofiles show strong enrichment within peaks and a weak positive correlation with crossover rate (Fig. 4A,B; Supplemental Fig. S15A,B). H3K27me3 ChIP-seq signal correlates strongly with DMC1/ASY1 peak crossover rate, as indicated by well-separated 95% confidence intervals around per-quantile mean coverage profiles (Fig. 4A,B; Supplemental Fig. S15A,B). A positive correlation with crossover rate is also evident for H3K27ac ChIP-seq signal, which is enriched within peaks (Fig. 4A,B; Supplemental Fig. S15A,B). In contrast, the constitutive heterochromatic mark H3K27me1 is anticorrelated with crossover rate at peaks (Fig. 4A,B; Supplemental Fig. S15A,B). These findings suggest that the co-occurrence of H3K27me3-marked facultative heterochromatin with meiotic DSBs and axis occupancy promotes crossover formation in wheat.

Crossover-active genes have elevated DMC1, ASY1, H3K27me3, and polymorphisms

To investigate the properties of genes in relation to crossover rate, we divided genes into four quantiles according to decreasing crossover rate (mean genes per quantile = 25,964) (Fig. 5A). Genes with elevated crossover rates exhibit higher DMC1 and ASY1 ChIP-seq signals on average (Fig. 5A). Equivalently, genes grouped according to higher DMC1 or ASY1 signals have higher crossover rates (Fig. 5B,C). DMC1 and ASY1 signals around genes are anticorrelated with nucleosome signal ($r_s = -0.42$ and -0.48, respectively) and are most depleted at the +1 nucleosome, where H3K4me3 ChIP-seq and MNase-seq signals are highest (Fig. 5A). Genes with higher DMC1 or ASY1 levels also have higher *Mariner* TE density in their promoter, transcribed, and downstream regions and higher *Mutator* density in their promoters (Supplemental Fig. S16A,B).

Similar to DMC1 and ASY1 peaks, gene crossover rate is positively correlated with H3K27me3 (Fig. 5A). In contrast, non-CG DNA methylation is anticorrelated with crossover rate (Fig. 5A), consistent with recombination suppression by DNA methylation (Yelina et al. 2015). Metaprofiles of RNA-seq coverage derived from anthers show that genes with higher crossover rates have lower meiotic expression on average (Fig. 5A; Martín et al. 2018). Gene crossover rate is also anticorrelated with H3K4me1 (Fig. 5A), a chromatin modification deposited within the transcribed regions of ubiquitously expressed housekeeping genes and in H3K27me3-depleted regions in *Arabidopsis* (Zhang et al. 2009). These findings are consistent with crossovers occurring more frequently around genes that are facultatively repressed via H3K27me3 and which also have elevated meiotic DSBs and axis occupancy.

To investigate levels of genetic variation in relation to recombination, we calculated metaprofiles of single-nucleotide polymorphism (SNP) density around genes grouped by crossover rate, DMC1, or ASY1 (Fig. 5A; Supplemental Fig. S16A,B). We analyzed SNPs identified among 811 geographically diverse cultivars and landraces, profiled via exome sequencing (He et al. 2019). Per-quantile metaprofiles reveal positive relationships for genic SNP density with crossover rate, DMC1, and ASY1 (Fig. 5A; Supplemental Fig. S16A,B), consistent with the mutagenic effects of meiotic recombination (Arbeithuber et al. 2015; Halldorsson et al. 2019). Additionally, we observed a negative relationship between crossover rate and the ratio of SNPs predicted to have a deleterious impact on protein function (dSNPs) to synonymous SNPs (sSNPs) ($\log_2$[dSNP/sSNP]) (Fig. 5A). This indicates more efficient purging of deleterious mutations from loci with elevated crossover rates, which is consistent with reduced genetic load in highly recombining regions of the wheat and maize genomes (Barton and Charlesworth 1998; Rodgers-Melnick et al. 2015; Jordan et al. 2018; He et al. 2019).

Gene function and transcriptional profile correlate with crossovers, DMC1, ASY1, and H3K27me3

We examined the functional annotation of genes grouped by decreasing crossover rate, DMC1, ASY1, or H3K27me3 by applying Gene Ontology term enrichment analysis to each quantile. Genes in the upper quantile for crossover rate or H3K27me3 are overrepresented for stress response and developmental annotations (Supplemental Tables S4, S5, S10, S11). These findings agree with previously reported functional stratification along the wheat chromosomes (IWGSC 2018; Ramírez-González et al. 2018). However, genes in the top quantile for DMC1 or ASY1 ChIP-seq exhibit a more heterogeneous functional composition, including overrepresentation of terms associated with housekeeping processes and meiosis, in addition to stress response and developmental annotations (Supplemental Tables S6–S9). This is consistent with the widespread distribution of DMC1 and ASY1 peaks along the chromosomes, including in crossover-suppressed regions.

Gene recombination and chromatin quantiles were next tested for over- and underrepresentation of gene categories using the hypergeometric distribution. Meiotic genes ($n = 1059$) are over- and underrepresented in the upper and lower quantiles, respectively, for DMC1 or ASY1 ChIP-seq signal (Fig. 6B,C; Supplemental Tables S17, S18; Alabdullah et al. 2019). Gene quantiles for crossover rate or H3K27me3 ChIP-seq signal show trends that are opposite to those for DMC1 and ASY1 with respect to meiotic genes (Fig. 6A,D; Supplemental Tables S16, S19). This attests to the functional heterogeneity of genes enriched for DMC1 and ASY1 and is consistent with the concentration of meiotic genes in crossover-suppressed regions (Alabdullah et al. 2019).

We evaluated gene quantiles for patterns of homoeologous gene expression, using previously defined categories derived from analysis of RNA-seq data from 15 tissues in Chinese Spring (Ramírez-González et al. 2018). This analysis applies to genes with a single identifiable homoeolog in each of the three subgenomes, which define gene triads (Ramírez-González et al. 2018). Stably and dynamically expressed triads are those in the bottom and top 10%, respectively, with regard to the mean of the Euclidean distances between relative transcript abundance for each tissue and the mean relative transcript abundance across all tissues (Ramírez-González et al. 2018). Balanced gene triads are those with comparable relative transcript abundances from each of the homoeologs, whereas dominant and suppressed categories refer to those with higher or lower transcript abundance from one homoeolog (Ramírez-González et al. 2018). The upper crossover-rate and H3K27me3 gene quantiles are overrepresented for dynamic and nonbalanced expression categories and underrepresented for stable and balanced categories, whereas opposite trends are observed for the lower quantiles (Fig. 6A,D; Supplemental Tables S12, S15). This is consistent with crossovers occurring preferentially in regions containing facultatively silenced genes with tissue-specific transcriptional profiles (Ramírez-González et al. 2018). DMC1 and ASY1 gene quantiles exhibit trends that are generally the inverse of those observed for crossover rate and H3K27me3 quantiles (Fig. 6B,C; Supplemental Tables S13, S14). Therefore, widespread meiotic DSB formation and axis occupancy occur beyond crossover-competent regions and around diverse gene categories.

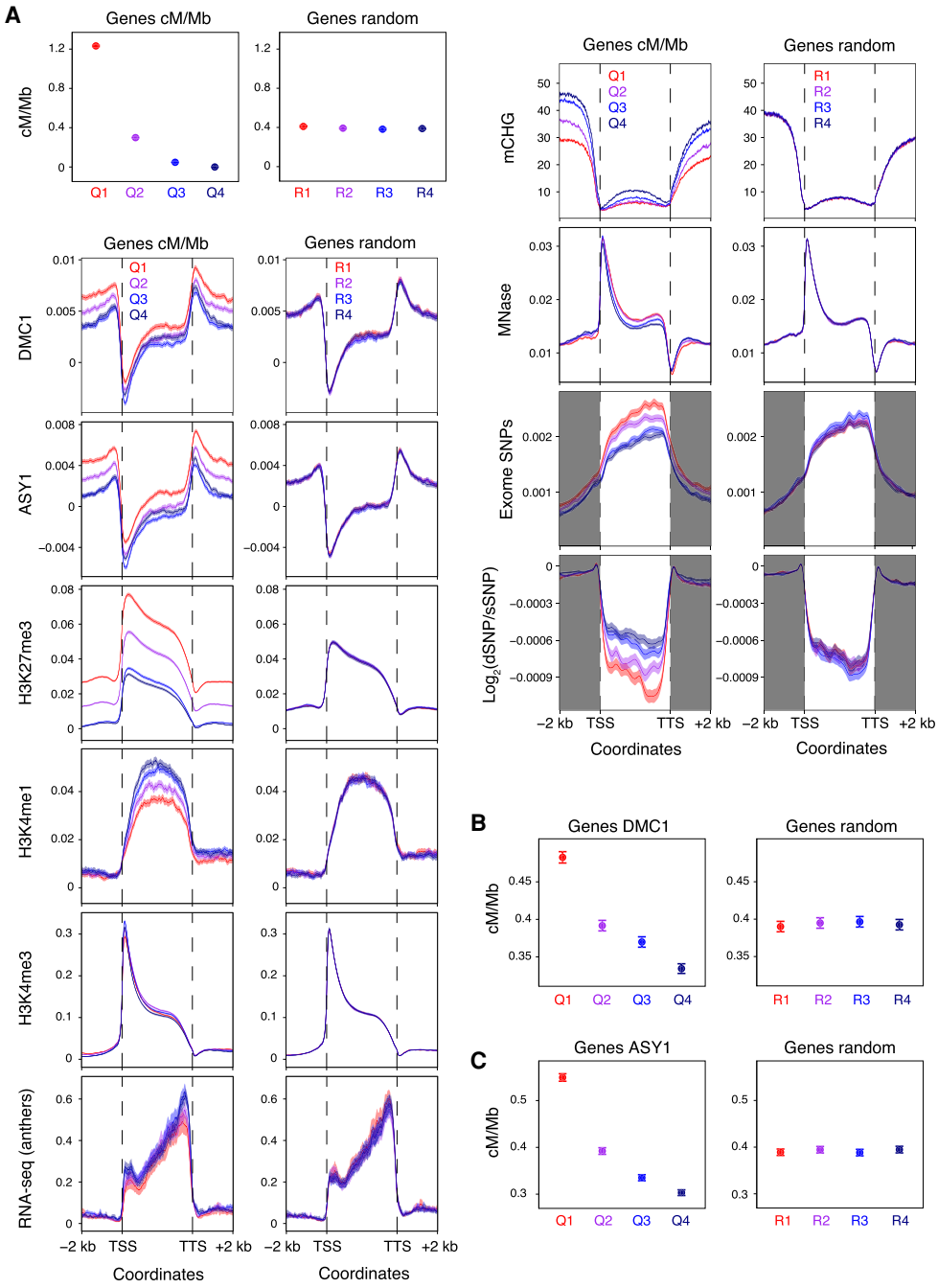

Figure 5. Patterns of genic recombination, chromatin, transcription, and polymorphism. (*A*) Genes were divided into four groups corresponding to those in the 100th–75th (Quantile 1), 75th–50th (Quantile 2), 50th–25th (Quantile 3), and 25th–0th (Quantile 4) percentiles with regard to their mean crossover rate (cM/Mb, derived from the Chinese Spring × Renan genetic map) between 1 kb upstream of transcriptional start sites (TSSs) and 1 kb downstream from transcriptional termination sites (TTSs) (Q1–Q4, *left*), or into four randomized groups (R1–R4, *right*). Solid circles denote the mean crossover rate for each group of genes (error bars = 95% confidence intervals for mean cM/Mb values). Metaprofiles show windowed mean values (solid lines) for each group of genes and 2-kb flanking regions (transparent ribbons = 95% confidence intervals). ChIP-seq coverage metaprofiles of DMC1, ASY1, H3K27me3 (IWGSC 2018), and H3K4me1 (Li et al. 2019) are derived from $\log_2$(ChIP/input) profiles, and those for H3K4me3 from $\log_2$(ChIP/MNase) profiles. Metaprofiles of RNA-seq coverage (transcripts per million, TPM) are derived from Chinese Spring anthers collected at the leptotene–zygotene transition (Martín et al. 2018). CHG-context DNA methylation (mCHG) metaprofiles are based on the proportion of cytosines that are methylated per CHG site, as detected in whole-genome bisulfite sequencing data (IWGSC 2018). Metaprofiles of exome-sequencing-derived SNPs are based on windowed SNP frequencies (He et al. 2019). Although the vast majority of SNPs detected using exome sequencing are located within gene bodies, these data also provide genotypes outside of transcribed regions. Therefore, SNPs outside of transcribed regions were retained for metaprofile calculation (gray shading). Windowed ratios of predicted deleterious SNPs to synonymous SNPs ($\log_2$[dSNP/sSNP]) were also used for metaprofile calculation. (*B*) Genes were divided into four quantiles according to decreasing mean DMC1 $\log_2$(ChIP/input) coverage between 1 kb upstream of TSSs and 1 kb downstream from TTSs (Q1–Q4, *left*), or into four randomized groups (R1–R4, *right*). Solid circles denote the mean crossover rate for each group of genes (error bars = 95% confidence intervals for mean cM/Mb values). (*C*) As in *B*, but with genes divided into four groups according to decreasing mean ASY1 $\log_2$(ChIP/input) coverage (Q1–Q4, *left*), or into four randomized groups (R1–R4, *right*).

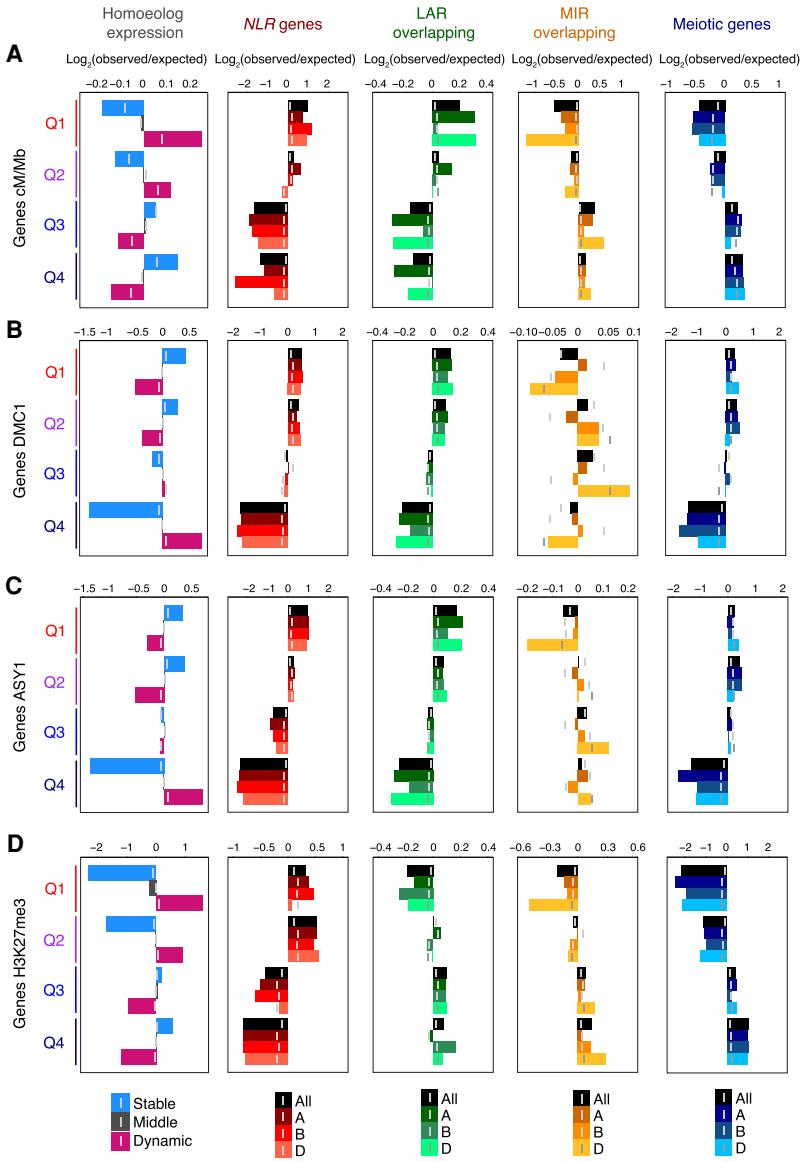

Figure 6. Gene expression pattern, function, and signatures of adaptation according to crossover rate, DMC1, ASY1, or H3K27me3. (*A*) Gene quantiles defined by decreasing mean crossover rate (Q1–Q4 = high–low cM/Mb) were evaluated for representation of (1) genes assigned to homoeolog expression categories (Homoeolog expression) (Ramírez-González et al. 2018), (2) genes encoding nucleotide-binding and leucine-rich repeat proteins (*NLR* genes) (Steuernagel et al. 2020), (3) genes overlapping genomic regions associated with local adaptation (LAR overlapping) (He et al. 2019), (4) genes overlapping genomic regions associated with modern wheat improvement (MIR overlapping) (He et al. 2019), and (5) genes with putative functions in meiosis (Meiotic genes) (Alabdullah et al. 2019). Log_2(observed/expected) ratios (bar graphs) and significance thresholds (vertical gray lines, $\alpha = 0.05$) were calculated by sampling from the hypergeometric distribution 100,000 times. Analyses were performed across all subgenomes and within each subgenome (All, A, B, and D). (*B*) As in *A*, but with genes divided into four quantiles according to decreasing mean DMC1 log_2(ChIP/input) coverage. (*C*) As in *A*, but with genes divided into four quantiles according to decreasing mean ASY1 log_2(ChIP/input) coverage. (*D*) As in *A*, but with genes divided into four quantiles according to decreasing mean H3K27me3 log_2(ChIP/input) coverage (IWGSC 2018).

To explore relationships between recombination and selection, we analyzed gene quantiles for overlap with genomic regions associated with local adaptation (LARs, $n = 42{,}918$, median width = 20 kb, LAR-overlapping genes = 33,247) (He et al. 2019). LARs were previously identified using a Bayesian method to test correlations between allele frequencies at 1.39 million exomic SNPs and 68 environmental and bioclimatic variables, for 26 geographically distinct wheat populations (He et al. 2019). LARs were defined as genomic regions containing locally adaptive SNPs (He et al. 2019). We observed that the upper gene quantiles for crossover rate, DMC1, and ASY1 are overrepresented for LAR overlap (Fig. 6A–C; Supplemental Tables S16–S18). We also evaluated quantiles for representation of genes overlapping genomic regions associated with the transition from landraces to modern improved cultivars (MIRs, $n = 4316$, median width = 350 kb, MIR-overlapping genes = 16,102), which were previously detected using nine regional populations (He et al. 2019). In contrast to genes overlapping LARs, MIR-overlapping genes are under- and overrepresented in the upper and lower quantiles for crossover rate, respectively, whereas these trends are not evident for genes ranked by DMC1 or ASY1 ChIP-seq (Fig. 6A–C; Supplemental Tables S16–S18). These relationships may reflect a role for crossovers in enabling selection for alleles conferring region-specific adaptive phenotypes, occurring since the global dissemination of hexaploid wheat. In contrast, overrepresentation of MIR-overlapping genes in the lower crossover-rate quantiles suggests that more recent agronomic gains achieved through selective breeding are associated with crossover-suppressed regions, consistent with recent analysis (Brinton et al. 2020).

NLR crossovers and clustering correlate with H3K27me3, DMCI, and ASYI

NLR genes are over- and underrepresented in the upper and lower quantiles, respectively, for crossover rate, DMC1, ASY1, and H3K27me3 (Fig. 6A–D; Supplemental Tables S16–S19). Upon recognition of pathogen virulence determinants, NLR proteins activate signal transduction pathways that precipitate hypersensitive cell death, as part of effector-triggered immunity (ETI) (Jones and Dangl 2006). *NLRs* are unevenly distributed throughout plant genomes and are frequently physically clustered, whereas others occur as singletons (Michelmore and Meyers 1998; Meyers et al. 2003). Among those detected in Chinese Spring (Steuernagel et al. 2020), 1233 *NLRs* exist in 328 physical clusters (mean per cluster = 3.76), whereas 473 are singletons. We divided *NLRs* into four quantiles, defined either by decreasing crossover rate (mean genes per quantile = 405) or by

decreasing cluster size (Quantile 4 contains only singletons; mean genes per quantile = 427) (Fig. 7A,B). *NLRs* with high and low crossover rates are over- and underrepresented for clustered genes, respectively, whereas inverse trends are evident for singletons (Fig. 7C; Supplemental Table S20). We also observed a positive correlation between *NLR* cluster size and crossover rate (Fig. 7B), consistent with recombination promoting cluster formation. The upper and lower quantiles for ASY1 and H3K27me3 ChIP-seq signal are over- and underrepresented for clustered *NLRs*, respectively, whereas opposite trends are apparent for singletons (Supplemental Fig. S17B; Supplemental Tables S22, S23). However, similar correlation with clustering is not evident for *NLRs* grouped by DMC1 ChIP-seq signal (Supplemental Fig. S17C; Supplemental Table S21).

Many *NLR* clusters comprise genes from the same phylogenetic clade, likely deriving from tandem duplications and intralocus recombination (Michelmore and Meyers 1998; Meyers et al. 2003). Heterogeneous *NLR* clusters containing genes from different clades also exist, indicative of segmental duplications and interlocus sequence exchange (Michelmore and Meyers 1998; Meyers et al. 2003). Using the wheat *NLR* phylogeny reported in Steuernagel et al. (2020), we found that 21% of physical clusters comprise *NLRs* whose most recent common ancestor is the parent node of at least one of the *NLRs* within their respective physical cluster. This provides a conservative estimate of *NLR* clusters that are monophyletic. Among *NLRs* in the upper and lower quantiles for crossover rate, we observed over- and underrepresentation of those that are members of monophyletic physical clusters, respectively (Supplemental Fig. S17D; Supplemental Table S20). This supports a role for intralocus crossover in the genesis of monophyletic clusters. *NLRs* with elevated crossover rates, or those within large physical clusters, also have higher H3K27me3 and, to lesser extents, higher DMC1 and ASY1 ChIP-seq signals (Fig. 7A,B). DMC1 and ASY1 show strongest enrichment toward the middle of *NLR* transcribed regions, as well as in promoters and at TTSs, patterns which are distinct from metaprofiles around all genes (Figs. 5A, 7A,B). Intragenic meiotic DSBs may provide the basis for duplications within the leucine-rich repeat (LRR)-encoding domains of plant *NLRs*, which

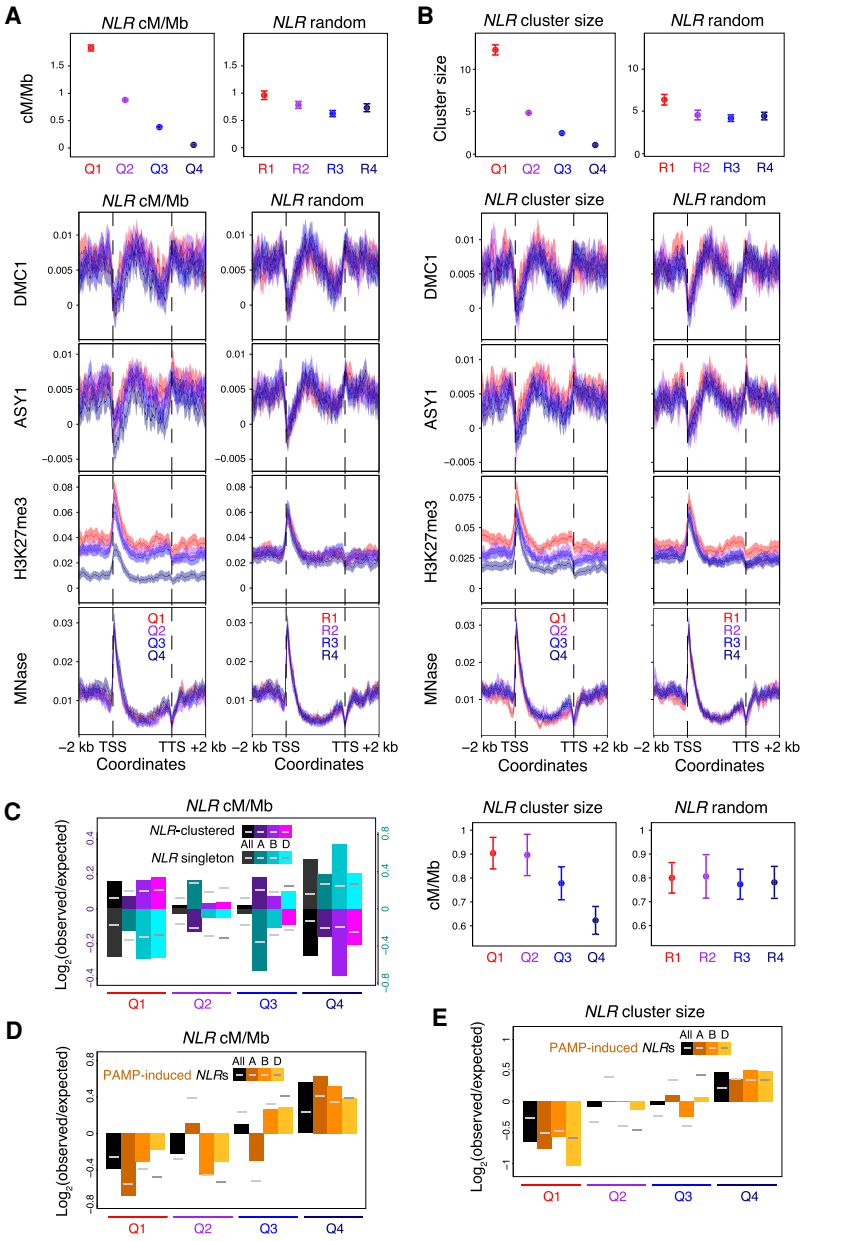

Figure 7. Chromatin, recombination, and clustering at nucleotide-binding and leucine-rich repeat (*NLR*) genes. (*A*) *NLR* genes were divided into four groups corresponding to those in the 100th–75th (Quantile 1), 75th–50th (Quantile 2), 50th–25th (Quantile 3), and 25th–0th (Quantile 4) percentiles with regard to their mean crossover rate (cM/Mb, derived from the Chinese Spring × Renan genetic map) between 1 kb upstream of transcriptional start sites and 1 kb downstream from transcriptional termination sites (Q1–Q4, *left*), or into four randomized groups (R1–R4, *right*). Solid circles denote the mean crossover rate for each group of genes (error bars = 95% confidence intervals for mean cM/Mb values). Metaprofiles show windowed mean values (solid lines) for each group of genes and 2-kb flanking regions (transparent ribbons = 95% confidence intervals). ChIP-seq coverage metaprofiles of DMC1, ASY1, and H3K27me3 (IWGSC 2018) are derived from $\log_2$(ChIP/input) profiles. (*B*) As in *A*, but with *NLR* genes divided into four groups according to decreasing physical cluster size (Q1–Q4, *left*), or into four randomized groups (R1–R4, *right*). Solid circles denote the mean cluster size (*upper* plots) or crossover rate (*lower* plots) for each group of genes (error bars = 95% confidence intervals for mean cluster size or cM/Mb values). (*C*) *NLR* gene quantiles defined by decreasing mean crossover rate (Q1–Q4 = high–low cM/Mb) were evaluated for representation of physically clustered or singleton *NLR* genes. Log_2(observed/expected) ratios (bar graphs) and significance thresholds (horizontal gray lines, $\alpha = 0.05$) were calculated by sampling from the hypergeometric distribution 100,000 times. Analyses were performed across all subgenomes and within each subgenome (All, A, B, and D). (*D*) As in *C*, but analyzing *NLR* gene quantiles defined by decreasing mean crossover rate for representation of *NLR* genes that were up-regulated upon challenge with pathogen-associated molecular patterns (PAMPs) (Steuernagel et al. 2020). (*E*) As in *D*, but analyzing *NLR* gene quantiles defined by decreasing physical cluster size.

have been proposed to arise from recombination (Parker et al. 1997).

Transmembrane pattern-recognition receptors (PRRs) mediate cell-surface perception of conserved microbial elicitors, termed pathogen-associated molecular patterns (PAMPs) (Jones and Dangl 2006). This process induces PAMP-triggered immunity (PTI), which can arrest infection by activating conserved plant defense pathways (Jones and Dangl 2006). Steuernagel et al. (2020) identified 266 wheat *NLRs* that were transcriptionally up-regulated upon challenge with PAMPs, indicating that PTI also regulates the expression of some *NLRs* as a primer for ETI induction. PAMP-induced *NLRs* are overrepresented among low-crossover-rate *NLRs* and singletons (Fig. 7D, E; Supplemental Tables S20, S24). Hence, *NLRs* that may operate at the interface between PTI and ETI concentrate in relatively crossover-suppressed regions.

DMC1 and ASY1 correlate with historical crossovers, nucleotide diversity, and signatures of selection

In view of the strong associations between contemporary crossovers, recombination initiation, polymorphism density, and genes with functional annotations related to adaptive traits, we investigated connections between DMC1, ASY1, historical crossovers, nucleotide diversity, and signatures of selection. We estimated historical recombination using per-gene R_M divided by gene width. R_M is the minimum number of crossovers in the history of a sample, based on the four-gamete test (Hudson and Kaplan 1985). For brevity, we present results for a population of 91 hexaploid wheat accessions sampled from Central, East, and South Asia (He et al. 2019), which are representative of findings for all regional populations. We divided genes into quantiles defined by decreasing R_M (mean genes per quantile = 25,066) or by decreasing DMC1 or ASY1 ChIP-seq signal (mean genes per quantile = 26,300) (Fig. 8A,B; Supplemental Fig. S18A). Two groups were defined for R_M due to the lower resolution of this statistic, which is limited by SNP density. We observed that elevated DMC1 and ASY1 levels associate with higher historical recombination (R_M) and nucleotide diversity (π) within genes (Fig. 8A,B; Supplemental Fig. S18A).

To investigate signatures of selection at genes as a function of recombination, we analyzed Tajima's *D* and composite likelihood ratios (CLRs) for each quantile (Tajima 1989; Nielsen et al. 2005). Tajima's *D* compares the number of segregating sites with nucleotide diversity, such that, under neutrality, *D* is assumed to be zero (Tajima 1989). Negative values of Tajima's *D* indicate directional selection or recent population expansion, whereas positive values indicate balancing selection or recent population contraction (Tajima 1989). We observed evidence for directional selection at high-recombination genes, with R_M, DMC1, and ASY1 each showing a negative relationship with Tajima's *D* (Fig. 8A,B; Supplemental Fig. S18A). CLRs provide a measure of directional selection that is more robust to varying recombination rate and demography, with higher values indicating the effects of selective sweeps (Nielsen et al. 2005). Positive relationships were observed for R_M, DMC1, and ASY1 with CLRs, indicating that signatures of selective sweeps are greater in high-recombination regions (Fig. 8A,B; Supplemental Fig. S18A). These findings suggest that loci with elevated recombination undergo more efficient selection for alleles conferring adaptive advantages.

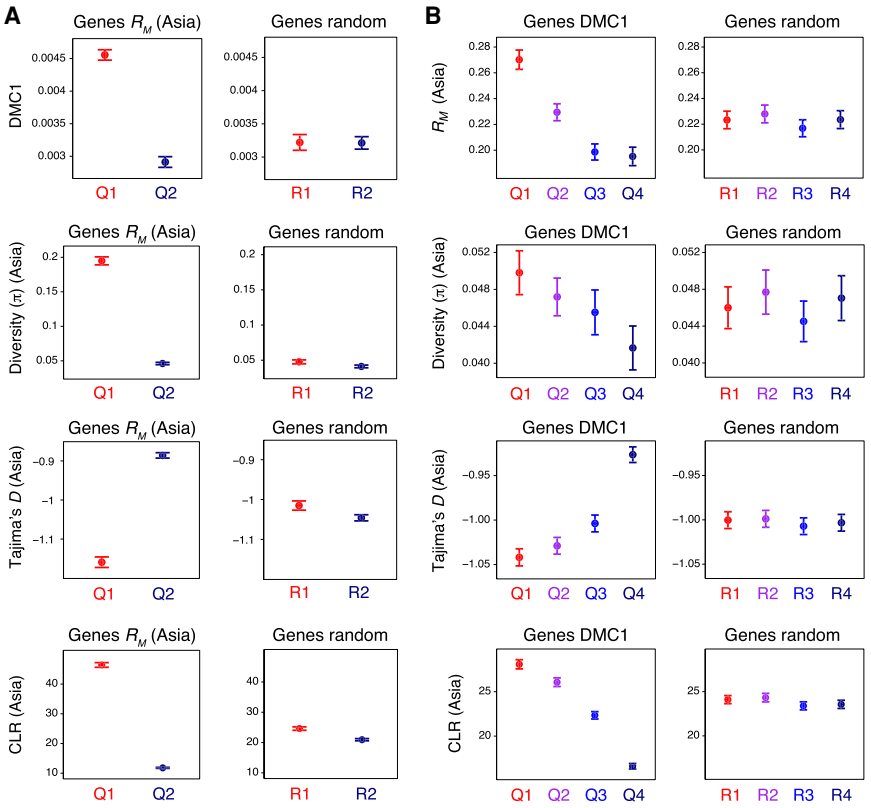

Figure 8. Historical recombination, DMC1, nucleotide diversity, and signatures of selection within genes. (*A*) Genes were divided into two groups corresponding to those in the 100th–50th (Quantile 1) and 50th–0th (Quantile 2) percentiles with regard to R_M divided by gene width (Q1–Q2, *left*), or into two randomized groups (R1–R2, *right*). R_M is the minimum number of crossovers that occurred in the history of a population of 91 hexaploid wheat accessions sampled from Central, East, and South Asia, inferred from genotypes at exome-sequencing-derived SNPs (He et al. 2019). Solid circles denote the mean value of the indicated parameter for each group of genes (error bars = 95% confidence intervals for mean values). Nucleotide diversity (the mean number of intrapopulation pairwise nucleotide differences per gene, π) was divided by gene width. Per-gene Tajima's *D* and composite likelihood ratios (CLRs) were also calculated. (*B*) As in *A*, but with genes divided into four groups according to decreasing mean DMC1 $\log_2$(ChIP/input) coverage (Q1–Q4, *left*), or into four randomized groups (R1–R4, *right*).

Discussion

This work provides the first nucleotide-resolution maps of the meiosis-specific recombinase DMC1, which marks resected meiotic DSBs, and the chromosome axis protein ASY1 in wheat. Using ChIP-seq, we observed co-enrichment of DMC1 and ASY1 in the crossover-active distal regions. Consonantly, we observed cytological immunolocalization of DMC1 and ASY1 close to the telomeres during early meiotic prophase I (Osman et al. 2021). DMC1 and ASY1 ChIP-seq signals associate with gene NDRs and TIR-containing DNA transposons. TIR-containing transposons insert

preferentially into gene regulatory sequences (Wicker et al. 2018) and have been widely associated with elevated meiotic recombination in plants (Yandeau-Nelson et al. 2005; Darrier et al. 2017; Marand et al. 2017; Choi et al. 2018). However, ASY1 ChIP-seq and nucleosome occupancy (MNase-seq) are positively correlated in *Arabidopsis* (Lambing et al. 2020). This may indicate contrasting relationships between the meiotic axis and chromatin in wheat and *Arabidopsis*. Alternatively, this may reflect differences in the stage of meiotic prophase analyzed by ChIP-seq.

Although DMC1 and ASY1 are distally enriched in wheat, we observed peaks along the length of each chromosome, including in crossover-suppressed compartments at lower densities. This is consistent with recent genetic maps, which revealed that gene conversion events were more evenly distributed than crossovers along the chromosomes (Gardiner et al. 2019). We therefore investigated DMC1 and ASY1 ChIP-seq peaks and genes for properties that distinguish those associated with elevated crossover rates. This revealed that the Polycomb histone modification H3K27me3, a marker of facultative heterochromatin, is one of the strongest predictors of crossover activity at these loci. Furthermore, this mark shows pronounced enrichment in the crossover-active distal regions. As H3K27me3 mediates transient and tissue-specific gene silencing during regulation of development and stress responses (Mozgova and Hennig 2015), this may reflect a coupling of crossovers to loci where elevated diversity and recombination are more likely to lead to adaptive benefits. Pedigree-based and population genetic analyses of recombination rates in human genomes have also associated H3K27me3 with higher local crossover rates (Halldorsson et al. 2019; Spence and Song 2019). However, it is important to note that differences in crossover formation between the wheat chromosome compartments are also connected to earlier homolog pairing and meiotic DSB formation that occur in cereal subtelomeric regions (Higgins et al. 2012; Osman et al. 2021). For example, crossover interference or post-translational modification of the axis proteins following crossover designation in distal regions could direct noncrossover outcomes for interstitial and centromere-proximal DSBs.

We observed positive relationships for genic sequence variation with both contemporary and historical crossover rates, as well as with DMC1 and ASY1 ChIP-seq signals. Recombination can break linkage between beneficial and deleterious mutations located on the same chromosome (Felsenstein 1974; Barton and Charlesworth 1998). For example, wheat and maize low-recombination regions carry a higher genetic load (Rodgers-Melnick et al. 2015; He et al. 2019), indicating that deleterious mutations are more efficiently removed from high-recombination regions. However, meiotic recombination is also mutagenic (Arbeithuber et al. 2015; Halldorsson et al. 2019), and positive relationships between nucleotide diversity and population-scaled recombination estimates have been observed in many plant and animal genomes (Begun and Aquadro 1992; Spencer et al. 2006; Gore et al. 2009; Cutter and Payseur 2013). Hence, elevated recombination may cause higher SNP levels due to mutational effects. Recombination also influences SNP maintenance within populations, by reducing linked selection between mutations (Hill and Robertson 1966; Barton and Charlesworth 1998). However, there is also a feedback on recombination, as very high levels of divergence, including structural changes, can strongly inhibit crossovers (Crown et al. 2018; Rowan et al. 2019). Our observations are consistent with crossovers accelerating evolution of distal loci by enabling more efficient selection for alleles conferring adaptive benefits (Hill and Robertson 1966; Barton and Charlesworth 1998). In contrast, reduced crossovers in the interstitial and centromere-proximal compartments may help preserve conserved functions of housekeeping and meiotic genes that are enriched in these regions (Akhunov et al. 2003).

We observed that genes with elevated crossover rates are overrepresented for those encoding NLR immunity proteins. Furthermore, *NLRs* with higher crossover rates show a greater degree of physical clustering, indicating that crossovers promote structural diversity at wheat *NLR* loci and thereby influence disease resistance. This is consistent with the Red Queen hypothesis that host sexual recombination provides adaptive benefits by generating novel genotypes that confer resistance to co-evolving parasites (Howard and Lively 1994; Brockhurst et al. 2014). Functional stratification of the wheat chromosomes is reminiscent of the "two-speed genome," which describes the bipartite genome organization of some plant-pathogenic oomycetes and fungi (Frantzeskakis et al. 2019). Virulence determinants in these pathogens are concentrated within fast-evolving, repeat-rich genomic compartments, separated from widely conserved housekeeping genes (Frantzeskakis et al. 2019). The mechanisms by which wheat and pathogen genomes have become compartmentalized are likely to be distinct, although these architectures may together promote co-evolutionary adaptation.

The plant immune system consists of two major layers. PAMP-triggered immunity provides species-level (nonhost) resistance to nonadapted pathogens (Dodds and Rathjen 2010). Within effector-triggered immunity, intracellular NLR disease resistance proteins often confer race-specific resistance effective against rapidly evolving virulence effectors, providing a second layer of defense (Jones and Dangl 2006). Wheat *NLR* genes that are transcriptionally induced following PAMP challenge have recently been identified (Steuernagel et al. 2020), consistent with crosstalk between PTI and ETI pathways (Ngou et al. 2021; Yuan et al. 2021). We observed that PAMP-induced *NLRs* occur more frequently as singletons located in low-crossover regions. PAMP-induced *NLRs* that may operate at the interface between PTI and ETI are therefore more insulated from the diversity-generating effects of crossovers. We speculate that *NLRs* that are induced during ETI may concentrate in more highly recombining regions, with novel resistance specificities and physical clustering arising from elevated crossovers. Hence, crossover patterns may be further stratified within the plant immune system. However, although clustered wheat *NLRs* tend to occur in higher crossover-rate regions compared to singletons, very large *NLR* clusters may constitute structural polymorphisms that inhibit crossover formation. For example, crossovers are suppressed by structural polymorphism at the *Arabidopsis RPP4–RPP5* and *RPP8* loci, the *Dm3* locus in lettuce, and the *I* locus in common bean (McDowell et al. 1998; Noël et al. 1999; Chin et al. 2001; Vallejos et al. 2006).

Our findings have relevance for wheat improvement through the deployment of genetic or epigenetic manipulations aimed at increasing crossover rates in recombination-suppressed chromosome compartments. For example, *Arabidopsis* DNA methyltransferase mutants show increased meiotic recombination within centromere-proximal regions (Choi et al. 2018; Underwood et al. 2018). Our work also points to the facultative heterochromatic mark H3K27me3 as a potential target for increasing crossovers. Chromatin modifications could be combined with *trans*-acting loci that direct crossovers to interstitial regions, which have recently been mapped in wheat (Jordan et al. 2018; Gardiner et al. 2019). Tools for promoting crossovers in these regions may have the potential to increase the efficiency of selection during breeding and accelerate adaptation to changing climates.

Methods

Western blotting and ChIP-seq

Western blotting and ChIP-seq were performed using standard protocols (Supplemental Methods). Pre-emergence spikes from wild-type Chinese Spring were crosslinked using formaldehyde, followed by nuclei purification and ChIP using α-DMC1 and α-ASY1 antibodies (Sanchez-Moran et al. 2007; Desjardins et al. 2020). Chromatin immunoprecipitation of the histone modifications H3K4me3 (Abcam ab8580), H3K9me2 (Abcam ab1220), and H3K27me1 (Sigma-Aldrich 07-448) was performed using a protocol similar to that described for DMC1 and ASY1 but using MNase digestion for chromatin fragmentation. MNase digestion was also applied without immunoprecipitation to generate a library for high-throughput sequencing (MNase-seq). DNA obtained from ChIP and MNase digestion was used to construct paired-end libraries, which were sequenced with 2 × 75-bp Illumina reads (Supplemental Methods).

Meiotic immunocytology

Chromosome spreads of pollen mother cells from the wheat cultivar Cadenza were immunostained for ASY1, DMC1, and H3K27me3 as described (Armstrong et al. 2002), with minor modifications (Supplemental Methods). Primary antibodies were used at the following dilutions: α-AtASY1 rabbit or guinea pig, 1:500 (Armstrong et al. 2002); α-AtDMC1 rabbit, 1:200 (Sanchez-Moran et al. 2007); and α-H3K27me3 rabbit, according to the manufacturer's guidelines (Diagenode C15310069 [CS-069-100]).

Short-read data alignment and processing

Deduplicated and trimmed paired-end ChIP-seq and MNase-seq reads were aligned to the RefSeq v1.0 Chinese Spring reference genome assembly (IWGSC 2018), using Bowtie 2 v2.3.4.3 (Supplemental Methods; Langmead and Salzberg 2012). Read pairs that aligned equally well to more than one genomic location, without a best-scoring alignment (with Bowtie 2-assigned MAPQ < 2), were discarded. For retained read pairs that aligned to multiple locations, with varying alignment scores, the best-scoring alignment was selected (Supplemental Table S1). Alignments with more than six mismatches or consisting of only one read in a pair were discarded. Additionally, alignment MAPQ and mismatch thresholds were varied to assess their impact on patterns of DMC1 and ASY1 ChIP-seq enrichment (Supplemental Methods; Supplemental Figs. S4–S9). Using the retained unique and multiple alignments combined in BAM format, windowed read counts per million mapped reads (CPM) were generated with the bamCoverage tool from deepTools v3.1.3 (Ramírez et al. 2014). Published bisulfite sequencing (IWGSC 2018) and RNA-seq (Martín et al. 2018) data were analyzed using standard workflows (Supplemental Methods).

ChIP-seq peak analysis

Sites of local ChIP-seq enrichment were identified by calling peaks using the ranger tool within PeakRanger v1.18 (Feng et al. 2011). Compartmentalized DMC1 and ASY1 ChIP-seq peak sets were evaluated for overlap with other genomic features using permutation tests implemented in regioneR v1.6.2, each utilizing 10,000 sets of randomly positioned loci of the same number and width distribution, and in the same genomic compartments, as the DMC1 or ASY1 peaks (Gel et al. 2016). These peak sets were also analyzed for overrepresented DNA sequence motifs using Weeder v2.0 (Supplemental Methods; Zambelli et al. 2014).

Fine-scale profiling of ChIP-seq peaks and genes

Per-feature windowed coverage profiles were calculated using the computeMatrix tool from deepTools v3.1.3 (Ramírez et al. 2014). CPM values for a ChIP input sequencing library (accessed from the NCBI Sequence Read Archive [SRA; https://www.ncbi.nlm.nih.gov/sra] accession SRR6350669) (IWGSC 2018), and for the MNase-seq library generated in the current study, were used in conjunction with those for ChIP-seq libraries derived from chromatin fragmented by sonication or by MNase digestion, respectively, to calculate windowed $\log_2([\text{ChIP}+1]/[\text{control}+1])$ coverage ratios for each chromosome or feature. Per-feature windowed SNP (He et al. 2019) and TE (IWGSC 2018) frequency profiles were calculated using the normalizeToMatrix function from the Bioconductor package EnrichedHeatmap v1.12.0 (Supplemental Methods; Gu et al. 2018).

DMC1 and ASY1 ChIP-seq peaks, genes, and *NLRs* (Steuernagel et al. 2020) were divided into quantiles according to decreasing mean crossover rate between 1 kb upstream of feature start sites and 1 kb downstream from end sites, using previously calculated crossover rates derived from a Chinese Spring × Renan F_6 genetic map (Supplemental Methods; IWGSC 2018). Genes were also divided into quantiles according to decreasing mean DMC1, ASY1, or H3K27me3 ChIP-seq signal ($\log_2[(\text{ChIP}+1)/(\text{input}+1)]$) within 1-kb-extended boundaries. Metaprofiles (windowed means and 95% confidence intervals) were calculated and plotted for each group of features in R v3.5.0 (R Core Team 2018). Gene quantiles were evaluated for over- and underrepresentation of functional and expression categories using topGO v2.32.0 (https://doi.org/10.18129/B9.bioc.topGO) and the hypergeometric distribution (Supplemental Methods). Published exome-sequencing-derived SNPs (He et al. 2019) were annotated with their predicted impact on protein function using SnpEff v4.3t (Cingolani et al. 2012) and analyzed using PopGenome v2.7.5 to compute population genetics statistics for each gene (Supplemental Methods; Pfeifer et al. 2014).

Software availability

Custom scripts used in the preparation of this paper are provided as Supplemental Code, and are also available at GitHub (at: https://ajtock.github.io/Wheat_DMC1_ASY1_paper/).

Data access

All raw sequencing data generated in this study have been deposited in the ArrayExpress database at EMBL-EBI (www.ebi.ac.uk/arrayexpress) under accession numbers E-MTAB-9632 (ChIP-seq) and E-MTAB-9633 (MNase-seq).

Competing interest statement

The authors declare no competing interests.

Acknowledgments

We thank Ksenia Krasileva (University of California, Berkeley), Jemima Brinton (Royal Botanic Gardens, Kew), and members of the Henderson laboratory for helpful discussions. Research was supported by a European Research Council (ERC) Consolidator Grant "SynthHotSpot," ERC Proof of Concept grant "HEIREC," Biotechnology and Biological Sciences Research Council (BBSRC) sLola grant BB/N002628/1, Leverhulme Trust grant RPG-2019-259, Agriculture and Agri-Food Canada/BBSRC International Wheat Yield Partnership BB/T004282/1, BBSRC Industrial Partnership Award grant BB/N007557/1 with Meiogenix, and a

BBSRC Doctoral Training Partnership iCASE studentship with Klein Wanzlebener Saatzucht (KWS).

Author contributions: A.J.T., D.M.H., K.O., E.S.-M., J.D.H., K.J.E., F.C.H.F., and I.R.H. designed the research. D.M.H., W.J., and K.O. performed experiments. K.O. interpreted cytological data. A.J.T. wrote software and performed computational analyses. C.U. provided advice on genetic map and polymorphism analyses. A.J.T., D.M.H., and I.R.H. wrote the manuscript.

References

Akhunov ED, Goodyear AW, Geng S, Qi LL, Echalier B, Gill BS, Miftahudin A, Gustafson JP, Lazo G, Chao S, et al. 2003. The organization and rate of evolution of wheat genomes are correlated with recombination rates along chromosome arms. *Genome Res* **13:** 753–763. doi:10.1101/gr.808603

Alabdullah AK, Borrill P, Martin AC, Ramirez-Gonzalez RH, Hassani-Pak K, Uauy C, Shaw P, Moore G. 2019. A co-expression network in hexaploid wheat reveals mostly balanced expression and lack of significant gene loss of homeologous meiotic genes upon polyploidization. *Front Plant Sci* **10:** 1325. doi:10.3389/fpls.2019.01325

Arbeithuber B, Betancourt AJ, Ebner T, Tiemann-Boege I. 2015. Crossovers are associated with mutation and biased gene conversion at recombination hotspots. *Proc Natl Acad Sci* **112:** 2109–2114. doi:10.1073/pnas.1416622112

Armstrong SJ, Caryl AP, Jones GH, Franklin FCH. 2002. Asy1, a protein required for meiotic chromosome synapsis, localizes to axis-associated chromatin in *Arabidopsis* and *Brassica*. *J Cell Sci* **115:** 3645–3655. doi:10.1242/jcs.00048

Barton NH, Charlesworth B. 1998. Why sex and recombination? *Science* **281:** 1986–1990. doi:10.1126/science.281.5385.1986

Begun DJ, Aquadro CF. 1992. Levels of naturally occurring DNA polymorphism correlate with recombination rates in *D. melanogaster*. *Nature* **356:** 519–520. doi:10.1038/356519a0

Brinton J, Ramirez-Gonzalez RH, Simmonds J, Wingen L, Orford S, Griffiths S, 10 Wheat Genome Project, Haberer G, Spannagl M, Walkowiak S, et al. 2020. A haplotype-led approach to increase the precision of wheat breeding. *Commun Biol* **3:** 712. doi:10.1038/s42003-020-01413-2

Brockhurst MA, Chapman T, King KC, Mank JE, Paterson S, Hurst GDD. 2014. Running with the Red Queen: the role of biotic conflicts in evolution. *Proc R Soc Biol Sci* **281:** 20141382. doi:10.1098/rspb.2014.1382

Chambon A, West A, Vezon D, Horlow C, De Muyt A, Chelysheva L, Ronceret A, Darbyshire AR, Osman K, Heckmann S, et al. 2018. Identification of ASYNAPTIC4, a component of the meiotic chromosome axis. *Plant Physiol* **178:** 233–246. doi:10.1104/pp.17.01725

Chin DB, Arroyo-Garcia R, Ochoa OE, Kesseli RV, Lavelle DO, Michelmore RW. 2001. Recombination and spontaneous mutation at the major cluster of resistance genes in lettuce (*Lactuca sativa*). *Genetics* **157:** 831–849. doi:10.1093/genetics/157.2.831

Choi K, Zhao X, Tock AJ, Lambing C, Underwood CJ, Hardcastle TJ, Serra H, Kim J, Cho HS, Kim J, et al. 2018. Nucleosomes and DNA methylation shape meiotic DSB frequency in *Arabidopsis thaliana* transposons and gene regulatory regions. *Genome Res* **28:** 532–546. doi:10.1101/gr.225599.117

Choulet F, Alberti A, Theil S, Glover N, Barbe V, Daron J, Pingault L, Sourdille P, Couloux A, Paux E, et al. 2014. Structural and functional partitioning of bread wheat chromosome 3B. *Science* **345:** 1249721. doi:10.1126/science.1249721

Cingolani P, Platts A, Wang LL, Coon M, Nguyen T, Wang L, Land SJ, Lu X, Ruden DM. 2012. A program for annotating and predicting the effects of single nucleotide polymorphisms, SnpEff: SNPs in the genome of *Drosophila melanogaster* strain w1118; iso-2; iso-3. *Fly (Austin)* **6:** 80–92. doi:10.4161/fly.19695

Cole F, Keeney S, Jasin M. 2010. Comprehensive, fine-scale dissection of homologous recombination outcomes at a hot spot in mouse meiosis. *Mol Cell* **39:** 700–710. doi:10.1016/j.molcel.2010.08.017

Concia L, Veluchamy A, Ramirez-Prado JS, Martin-Ramirez A, Huang Y, Perez M, Domenichini S, Rodriguez Granados NY, Kim S, Blein T, et al. 2020. Wheat chromatin architecture is organized in genome territories and transcription factories. *Genome Biol* **21:** 104. doi:10.1186/s13059-020-01998-1

Crown KN, Miller DE, Sekelsky J, Hawley RS. 2018. Local inversion heterozygosity alters recombination throughout the genome. *Curr Biol* **28:** 2984–2990.e3. doi:10.1016/j.cub.2018.07.004

Cutter AD, Payseur BA. 2013. Genomic signatures of selection at linked sites: unifying the disparity among species. *Nat Rev Genet* **14:** 262–274. doi:10.1038/nrg3425

Darrier B, Rimbert H, Balfourier F, Pingault L, Josselin A-A, Servin B, Navarro J, Choulet F, Paux E, Sourdille P. 2017. High-resolution mapping of crossover events in the hexaploid wheat genome suggests a universal recombination mechanism. *Genetics* **206:** 1373–1388. doi:10.1534/genetics.116.196014

Demirci S, van Dijk ADJ, Sanchez Perez G, Aflitos SA, de Ridder D, Peters SA. 2017. Distribution, position and genomic characteristics of crossovers in tomato recombinant inbred lines derived from an interspecific cross between *Solanum lycopersicum* and *Solanum pimpinellifolium*. *Plant J* **89:** 554–564. doi:10.1111/tpj.13406

Desjardins SD, Ogle DE, Ayoub MA, Heckmann S, Henderson IR, Edwards KJ, Higgins JD. 2020. *MutS homologue 4* and *MutS homologue 5* maintain the obligate crossover in wheat despite stepwise gene loss following polyploidization. *Plant Physiol* **183:** 1545–1558. doi:10.1104/pp.20.00534

Dodds PN, Rathjen JP. 2010. Plant immunity: towards an integrated view of plant-pathogen interactions. *Nat Rev Genet* **11:** 539–548. doi:10.1038/nrg2812

Felsenstein J. 1974. The evolutionary advantage of recombination. *Genetics* **78:** 737–756. doi:10.1093/genetics/78.2.737

Feng X, Grossman R, Stein L. 2011. PeakRanger: a cloud-enabled peak caller for ChIP-seq data. *BMC Bioinformatics* **12:** 139. doi:10.1186/1471-2105-12-139

Ferdous M, Higgins JD, Osman K, Lambing C, Roitinger E, Mechtler K, Armstrong SJ, Perry R, Pradillo M, Cuñado N, et al. 2012. Inter-homolog crossing-over and synapsis in *Arabidopsis* meiosis are dependent on the chromosome axis protein AtASY3. *PLoS Genet* **8:** e1002507. doi:10.1371/journal.pgen.1002507

Frantzeskakis L, Kusch S, Panstruga R. 2019. The need for speed: compartmentalized genome evolution in filamentous phytopathogens. *Mol Plant Pathol* **20:** 3–7. doi:10.1111/mpp.12738

Fuentes R, Hesselink T, Nieuwenhuis R, Bakker L, Schijlen E, van Dooijeweert W, Diaz Trivino S, de Haan JR, Sanchez Perez G, Zhang X, et al. 2020. Meiotic recombination profiling of interspecific hybrid F1 tomato pollen by linked read sequencing. *Plant J* **102:** 480–492. doi:10.1111/tpj.14640

Gardiner LJ, Wingen LU, Bailey P, Joynson R, Brabbs T, Wright J, Higgins JD, Hall N, Griffiths S, Clavijo BJ, et al. 2019. Analysis of the recombination landscape of hexaploid bread wheat reveals genes controlling recombination and gene conversion frequency. *Genome Biol* **20:** 69. doi:10.1186/s13059-019-1675-6

Gel B, Díez-Villanueva A, Serra E, Buschbeck M, Peinado MA, Malinverni R. 2016. regioneR: an R/Bioconductor package for the association analysis of genomic regions based on permutation tests. *Bioinformatics* **32:** 289–291. doi:10.1093/bioinformatics/btv562

Gore MA, Chia J-MJ-M, Elshire RJ, Sun Q, Ersoz ES, Hurwitz BL, Peiffer JA, McMullen MD, Grills GS, Ross-Ibarra J, et al. 2009. A first-generation haplotype map of maize. *Science* **326:** 1115–1117. doi:10.1126/science.1177837

Gu Z, Eils R, Schlesner M, Ishaque N. 2018. EnrichedHeatmap: an R/Bioconductor package for comprehensive visualization of genomic signal associations. *BMC Genomics* **19:** 234. doi:10.1186/s12864-018-4625-x

Guo X, Su H, Shi Q, Fu S, Wang J, Zhang X, Hu Z, Han F. 2016. *De novo* centromere formation and centromeric sequence expansion in wheat and its wide hybrids. *PLoS Genet* **12:** e1005997. doi:10.1371/journal.pgen.1005997

Halldorsson BV, Palsson G, Stefansson OA, Jonsson H, Hardarson MT, Eggertsson HP, Gunnarsson B, Oddsson A, Halldorsson GH, Zink F, et al. 2019. Human genetics: characterizing mutagenic effects of recombination through a sequence-level genetic map. *Science* **363:** eaau1043. doi:10.1126/science.aau1043

He Y, Wang M, Dukowic-Schulze S, Zhou A, Tiang C-L, Shilo S, Sidhu GK, Eichten S, Bradbury P, Springer NM, et al. 2017. Genomic features shaping the landscape of meiotic double-strand-break hotspots in maize. *Proc Natl Acad Sci* **114:** 12231–12236. doi:10.1073/pnas.1713225114

He F, Pasam R, Shi F, Kant S, Keeble-Gagnere G, Kay P, Forrest K, Fritz A, Hucl P, Wiebe K, et al. 2019. Exome sequencing highlights the role of wild-relative introgression in shaping the adaptive landscape of the wheat genome. *Nat Genet* **51:** 896–904. doi:10.1038/s41588-019-0382-2

Higgins JD, Perry RM, Barakate A, Ramsay L, Waugh R, Halpin C, Armstrong SJ, Franklin FCH. 2012. Spatiotemporal asymmetry of the meiotic program underlies the predominantly distal distribution of meiotic crossovers in barley. *Plant Cell* **24:** 4096–4109. doi:10.1105/tpc.112.102483

Hill WG, Robertson A. 1966. The effect of linkage on limits to artificial selection. *Genet Res* **8:** 269–294. doi:10.1017/S0016672300010156

Howard RS, Lively CM. 1994. Parasitism, mutation accumulation and the maintenance of sex. *Nature* **367:** 554–557. doi:10.1038/367554a0

Hudson RR, Kaplan NL. 1985. Statistical properties of the number of recombination events in the history of a sample of DNA sequences. *Genetics* **111:** 147–164. doi:10.1093/genetics/111.1.147

Hunter N. 2015. Meiotic recombination: the essence of heredity. *Cold Spring Harb Perspect Biol* **7:** a016618. doi:10.1101/cshperspect.a016618

IWGSC. 2018. Shifting the limits in wheat research and breeding using a fully annotated reference genome. *Science* **361:** eaar7191. doi:10.1126/science.aar7191

Jones JDG, Dangl JL. 2006. The plant immune system. *Nature* **444:** 323–329. doi:10.1038/nature05286

Jordan KW, Wang S, He F, Chao S, Lun Y, Paux E, Sourdille P, Sherman J, Akhunova A, Blake NK, et al. 2018. The genetic architecture of genome-wide recombination rate variation in allopolyploid wheat revealed by nested association mapping. *Plant J* **95:** 1039–1054. doi:10.1111/tpj.14009

Keeney S, Lange J, Mohibullah N. 2014. Self-organization of meiotic recombination initiation: general principles and molecular pathways. *Annu Rev Genet* **48:** 187–214. doi:10.1146/annurev-genet-120213-092304

Lambing C, Kuo PC, Tock AJ, Topp SD, Henderson IR. 2020. ASY1 acts as a dosage-dependent antagonist of telomere-led recombination and mediates crossover interference in *Arabidopsis*. *Proc Natl Acad Sci* **117:** 13647–13658. doi:10.1073/pnas.1921055117

Langmead B, Salzberg SL. 2012. Fast gapped-read alignment with Bowtie 2. *Nat Methods* **9:** 357–359. doi:10.1038/nmeth.1923

Li Z, Wang M, Lin K, Xie Y, Guo J, Ye L, Zhuang Y, Teng W, Ran X, Tong Y, et al. 2019. The bread wheat epigenomic map reveals distinct chromatin architectural and evolutionary features of functional genetic elements. *Genome Biol* **20:** 139. doi:10.1186/s13059-019-1746-8

Liu Y, Yuan J, Jia G, Ye W, Jeffrey Chen Z, Song Q. 2021. Histone H3K27 dimethylation landscapes contribute to genome stability and genetic recombination during wheat polyploidization. *Plant J* **105:** 678–690. doi:10.1111/tpj.15063

Marand AP, Jansky SH, Zhao H, Leisner CP, Zhu X, Zeng Z, Crisovan E, Newton L, Hamernik AJ, Veilleux RE, et al. 2017. Meiotic crossovers are associated with open chromatin and enriched with *Stowaway* transposons in potato. *Genome Biol* **18:** 203. doi:10.1186/s13059-017-1326-8

Marcussen T, Sandve SR, Heier L, Spannagl M, Pfeifer M, International Wheat Genome Sequencing Consortium, Jakobsen KS, Wulff BBH, Steuernagel B, Mayer KFX, et al. 2014. Ancient hybridizations among the ancestral genomes of bread wheat. *Science* **345:** 1250092. doi:10.1126/science.1250092

Martín AC, Borrill P, Higgins J, Alabdullah A, Ramírez-González RH, Swarbreck D, Uauy C, Shaw P, Moore G. 2018. Genome-wide transcription during early wheat meiosis is independent of synapsis, ploidy level, and the *Ph1* locus. *Front Plant Sci* **9:** 1791. doi:10.3389/fpls.2018.01791

McDowell JM, Dhandaydham M, Long TA, Aarts MG, Goff S, Holub EB, Dangl JL. 1998. Intragenic recombination and diversifying selection contribute to the evolution of downy mildew resistance at the *RPP8* locus of *Arabidopsis*. *Plant Cell* **10:** 1861–1874. doi:10.1105/tpc.10.11.1861

Mercier R, Mézard C, Jenczewski E, Macaisne N, Grelon M. 2015. The molecular biology of meiosis in plants. *Annu Rev Plant Biol* **66:** 297–327. doi:10.1146/annurev-arplant-050213-035923

Meyers BC, Kozik A, Griego A, Kuang H, Michelmore RW. 2003. Genome-wide analysis of NBS-LRR–encoding genes in *Arabidopsis*. *Plant Cell* **15:** 809–834. doi:10.1105/tpc.009308

Michelmore RW, Meyers BC. 1998. Clusters of resistance genes in plants evolve by divergent selection and a birth-and-death process. *Genome Res* **8:** 1113–1130. doi:10.1101/gr.8.11.1113

Mozgova I, Hennig L. 2015. The Polycomb group protein regulatory network. *Annu Rev Plant Biol* **66:** 269–296. doi:10.1146/annurev-arplant-043014-115627

Ngou BPM, Ahn HK, Ding P, Jones JDG. 2021. Mutual potentiation of plant immunity by cell-surface and intracellular receptors. *Nature* **592:** 110–115. doi:10.1038/s41586-021-03315-7

Nielsen R, Williamson S, Kim Y, Hubisz MJ, Clark AG, Bustamante C. 2005. Genomic scans for selective sweeps using SNP data. *Genome Res* **15:** 1566–1575. doi:10.1101/gr.4252305

Noël L, Moores TL, van Der Biezen EA, Parniske M, Daniels MJ, Parker JE, Jones JD. 1999. Pronounced intraspecific haplotype divergence at the *RPP5* complex disease resistance locus of *Arabidopsis*. *Plant Cell* **11:** 2099–2112. doi:10.1105/tpc.11.11.2099

Osman K, Algopishi U, Higgins JD, Henderson IR, Edwards KJ, Franklin FCH, Sanchez-Moran E. 2021. Distal bias of meiotic crossovers in hexaploid bread wheat reflects spatio-temporal asymmetry of the meiotic program. *Front Plant Sci* **12:** 631323. doi:10.3389/fpls.2021.631323

Parker JE, Coleman MJ, Szabò V, Frost LN, Schmidt R, van der Biezen EA, Moores T, Dean C, Daniels MJ, Jones JD. 1997. The *Arabidopsis* downy mildew resistance gene RPP5 shares similarity to the toll and interleukin-1 receptors with N and L6. *Plant Cell* **9:** 879–894. doi:10.1105/tpc.9.6.879

Pfeifer B, Wittelsbürger U, Ramos-Onsins SE, Lercher MJ. 2014. PopGenome: an efficient Swiss army knife for population genomic analyses in R. *Mol Biol Evol* **31:** 1929–1936. doi:10.1093/molbev/msu136

Ramírez F, Dündar F, Diehl S, Grüning BA, Manke T. 2014. deepTools: a flexible platform for exploring deep-sequencing data. *Nucleic Acids Res* **42:** W187–W191. doi:10.1093/nar/gku365

Ramírez-González RH, Borrill P, Lang D, Harrington SA, Brinton J, Venturini L, Davey M, Jacobs J, Van Ex F, Pasha A, et al. 2018. The transcriptional landscape of polyploid wheat. *Science* **361:** eaar6089. doi:10.1126/science.aar6089

R Core Team. 2018. *R: a language and environment for statistical computing*. R Foundation for Statistical Computing, Vienna. https://www.R-project.org/.

Rodgers-Melnick E, Bradbury PJ, Elshire RJ, Glaubitz JC, Acharya CB, Mitchell SE, Li C, Li Y, Buckler ES. 2015. Recombination in diverse maize is stable, predictable, and associated with genetic load. *Proc Natl Acad Sci* **112:** 3823–3828. doi:10.1073/pnas.1413864112

Rowan BA, Heavens D, Feuerborn TR, Tock AJ, Henderson IR, Weigel D. 2019. An ultra high-density *Arabidopsis thaliana* crossover map that refines the influences of structural variation and epigenetic features. *Genetics* **213:** 771–787. doi:10.1534/genetics.119.302406

Saintenac C, Falque M, Martin OC, Paux E, Feuillet C, Sourdille P. 2009. Detailed recombination studies along chromosome 3B provide new insights on crossover distribution in wheat (*Triticum aestivum* L.). *Genetics* **181:** 393–403. doi:10.1534/genetics.108.097469

Sanchez-Moran E, Santos J-L, Jones GH, Franklin FCH. 2007. ASY1 mediates AtDMC1-dependent interhomolog recombination during meiosis in *Arabidopsis*. *Genes Dev* **21:** 2220–2233. doi:10.1101/gad.439007

Shilo S, Melamed-Bessudo C, Dorone Y, Barkai N, Levy AA. 2015. DNA crossover motifs associated with epigenetic modifications delineate open chromatin regions in *Arabidopsis*. *Plant Cell* **27:** 2427–2436. doi:10.1105/tpc.15.00391

Spence JP, Song YS. 2019. Inference and analysis of population-specific fine-scale recombination maps across 26 diverse human populations. *Sci Adv* **5:** eaaw9206. doi:10.1126/sciadv.aaw9206

Spencer CCA, Deloukas P, Hunt S, Mullikin J, Myers S, Silverman B, Donnelly P, Bentley D, McVean G. 2006. The influence of recombination on human genetic diversity. *PLoS Genet* **2:** e148. doi:10.1371/journal.pgen.0020148

Steuernagel B, Witek K, Krattinger SG, Ramirez-Gonzalez RH, Schoonbeek HJ, Yu G, Baggs E, Witek AI, Yadav I, Krasileva KV, et al. 2020. The NLR-annotator tool enables annotation of the intracellular immune receptor repertoire. *Plant Physiol* **183:** 468–482. doi:10.1104/pp.19.01273

Taagen E, Bogdanove AJ, Sorrells ME. 2020. Counting on crossovers: controlled recombination for plant breeding. *Trends Plant Sci* **25:** 455–465. doi:10.1016/j.tplants.2019.12.017

Tajima F. 1989. Statistical method for testing the neutral mutation hypothesis by DNA polymorphism. *Genetics* **123:** 585–595. doi:10.1093/genetics/123.3.585

Underwood CJ, Choi K, Lambing C, Zhao X, Serra H, Borges F, Simorowski J, Ernst E, Jacob Y, Henderson IR, et al. 2018. Epigenetic activation of meiotic recombination near *Arabidopsis thaliana* centromeres via loss of H3K9me2 and non-CG DNA methylation. *Genome Res* **28:** 519–531. doi:10.1101/gr.227116.117

Vallejos CE, Astua-Monge G, Jones V, Plyler TR, Sakiyama NS, Mackenzie SA. 2006. Genetic and molecular characterization of the I locus of *Phaseolus vulgaris*. *Genetics* **172:** 1229–1242. doi:10.1534/genetics.105.050815

Villeneuve AM, Hillers KJ. 2001. Whence meiosis? *Cell* **106:** 647–650. doi:10.1016/S0092-8674(01)00500-1

Wicker T, Gundlach H, Spannagl M, Uauy C, Borrill P, Ramírez-González RH, De Oliveira R, Mayer KFX, Paux E, Choulet F. 2018. Impact of transposable elements on genome structure and evolution in bread wheat. *Genome Biol* **19:** 103. doi:10.1186/s13059-018-1479-0

Yandeau-Nelson MD, Zhou Q, Yao H, Xu X, Nikolau BJ, Schnable PS. 2005. *MuDR* transposase increases the frequency of meiotic crossovers in the vicinity of a *Mu* insertion in the maize *a1* gene. *Genetics* **169:** 917–929. doi:10.1534/genetics.104.035089

Yelina NE, Lambing C, Hardcastle TJ, Zhao X, Santos B, Henderson IR. 2015. DNA methylation epigenetically silences crossover hot spots and controls chromosomal domains of meiotic recombination in *Arabidopsis*. *Genes Dev* **29:** 2183–2202. doi:10.1101/gad.270876.115

Yuan M, Jiang Z, Bi G, Nomura K, Liu M, Wang Y, Cai B, Zhou JM, He SY, Xin XF. 2021. Pattern-recognition receptors are required for NLR-mediated plant immunity. *Nature* **592:** 105–109. doi:10.1038/s41586-021-03316-6

Zambelli F, Pesole G, Pavesi G. 2014. Using Weeder, Pscan, and PscanChIP for the discovery of enriched transcription factor binding site motifs in nucleotide sequences. *Curr Protoc Bioinforma* **47:** 2.11.1–31. doi:10.1002/0471250953.bi0211s47

Zhang X, Bernatavichute YV, Cokus S, Pellegrini M, Jacobsen SE. 2009. Genome-wide analysis of mono-, di- and trimethylation of histone H3 lysine 4 in *Arabidopsis thaliana*. *Genome Biol* **10:** R62. doi:10.1186/gb-2009-10-6-r62

Zickler D, Kleckner N. 1999. Meiotic chromosomes: integrating structure and function. *Annu Rev Genet* **33:** 603–754. doi:10.1146/annurev.genet.33.1.603

Received November 3, 2020; accepted in revised form July 20, 2021.